Exceptional rings protected by emergent symmetry for mechanical systems

Tsuneya Yoshida and Yasuhiro Hatsugai

Department of Physics, University of Tsukuba, Ibaraki 305-8571, Japan

We propose mechanical systems, described by Newton's equation of motion, as suited platforms for symmetry protection of non-Hermitian degeneracies. We point out that in contrast to other systems with gain and loss, fine tuning of parameters is not required to realize symmetry-protected non-Hermitian degeneracies due to an emergent property of mechanical systems. The presence of symmetry-protected exceptional rings with extended chiral symmetry is numerically demonstrated for a mechanical graphene with friction. Furthermore, classification of symmetry-protected non-Hermitian degeneracies is addressed by taking into account the emergent properties of mechanical systems.

I. INTRODUCTION

After the discovery of a topological insulator for a quantum well of HgTe/CdTe [1–3], topological phenomena have been analyzed extensively [4,5]. Interestingly, topological phenomena can be observed even for classical systems. For instance, topologically protected excitations are reported for classical systems described by the Newton's law [6–8]. Other representative examples are systems described by the Maxwell's equations, e.g., photonic crystals [9–11] and electric circuits [12–14]. In particular, chiral edge states [15–17] realized for photonic crystals [11] provide the basis for novel devices (e.g., directional filters [18]), which enhances the significance of classical topological systems. The above topological phenomena both for quantum and classical systems are mathematically described as an eigenvalue problem of a Hermitian matrix.

Recently, theoretical and experimental efforts have opened a new field of research, non-Hermitian topological systems, where the eigenvalue problem becomes non-Hermitian [19–21]. The non-Hermitian topological phenomena have been reported for a variety of systems, such as open quantum systems [22–26], photonic crystals [27–33], and correlated systems in equilibrium, etc. [34–36]. In this field, as well as the bulk-edge correspondence under the non-Hermitian skin effect [37–42], the interplay between symmetry and the non-Hermiticity has been addressed as a central issue. In particular, the non-Hermiticity unifies [43,44] and ramifies [45] the symmetry classes. Furthermore, recent theoretical studies [46–48] have revealed that symmetry enriches the topology of exceptional points which arise from defectiveness of the Hamiltonian [25,49] (i.e., the breakdown of its diagonalizability). These novel non-Hermitian degeneracies are referred to as symmetry-protected exceptional rings (SPERs) for two-dimensional systems and symmetry-protected exceptional surfaces (SPESs) for three-dimensional systems.

So far, open quantum systems [22–26] and photonic systems [27–32] have mainly been analyzed as the experimental platforms of the non-Hermitian topological physics. In these systems, fine tuning is required in experiments to analyze the interplay of symmetry and non-Hermiticity, such as emergence of the aforementioned symmetry-protected non-Hermitian degeneracies. For example, to preserve parity-time symmetry (PT symmetry) in photonic systems, one needs to tune gain and loss as well as coupling between sites [50,51]. Therefore, for experimental realizations of symmetry-protected non-Hermitian degeneracies, it is important to find a system where relevant symmetry is preserved without fine tuning.

We here elucidate that without fine tuning, mechanical systems host symmetry-protected non-Hermitian topological degeneracies with extended chiral symmetry, which is an emergent property of the mechanical systems. Specifically, we demonstrate the presence of SPERs with extended chiral symmetry [48] for a mechanical graphene with homogeneous fiction. Interestingly, in such a system, the zeroth Chern number characterizing the SPERs can be obtained by experimental observable quantities. Furthermore, we also carried out topological classification of symmetry-protected non-Hermitian degeneracies by taking into account emergent properties of mechanical systems. The obtained result elucidates the robustness of SPERs in the mechanical graphene; SPERs survive even when the system is rotated because of the presence of *CP* symmetry, while SPERs vanish further breaking the inversion symmetry with inhomogeneous potentials arising from gravity.

The rest of this paper is organized as follows. In Sec. II, we elucidate that mechanical systems with friction host symmetry-protected non-Hermitian degeneracies with the emergent symmetry by recasting the equation of motion as an eigenvalue problem of a non-Hermitian matrix. In Sec. III, we demonstrate the emergence of SPERs with extended chiral symmetry for the mechanical graphene with homogeneous friction. In Sec. IV, we address topological classification of symmetry-protected non-Hermitian topological degeneracies by taking into account the special characteristics of mechanical systems.

II. SYMMETRY-PROTECTED NON-HERMITIAN DEGENERACIES WITH EMERGENT SYMMETRY

First, we show that a wide variety of mechanical systems host symmetry-protected non-Hermitian degeneracies, such as SPERs in two dimensions. Consider a mechanical system with friction where internal forces (e.g., the Coriolis force) and the Lorentz force are absent. In this case, the system preserves emergent symmetry (4) which results in the above symmetry-protected non-Hermitian degeneracies.

In the following, we discuss the symmetry of the systems and discuss the symmetry protection of the non-Hermitian degeneracies.

A. Matrix form of equation of motion

Let us consider a mechanical system, such as a coupled vibration system. Then, the equation of motion is given by

$$\ddot{u}_{\boldsymbol{k}}^{\mu} = -D^{\mu\nu}(\boldsymbol{k})u_{\boldsymbol{k}}^{\nu} + \Gamma_0^{\mu\nu}(\boldsymbol{k})\dot{u}_{\boldsymbol{k}}^{\nu}, \tag{1}$$

where $u_{\boldsymbol{k}}^{\mu}$ denotes the Fourier transformed displacement $(\mu, \nu = x, y)$ $\dot{u}_{\boldsymbol{k}}^{\mu} := \frac{du_{\boldsymbol{k}}^{\mu}}{dt}$. Summation over repeating indices is assumed. The first and second terms describe the potential force and the force proportional to the velocity.

In the matrix form, the above equation is rewritten as

$$\dot{\boldsymbol{\phi}}_{\boldsymbol{k}}(t) = M(\boldsymbol{k})\boldsymbol{\phi}_{\boldsymbol{k}}(t), \tag{2a}$$

$$M(\boldsymbol{k}) = \begin{pmatrix} 0 & \mathbb{1} \\ -D(\boldsymbol{k}) & \Gamma_0(\boldsymbol{k}) \end{pmatrix}_{\rho}, \tag{2b}$$

with $\boldsymbol{\phi}(t) = (\boldsymbol{u}_{\boldsymbol{k}} \quad \dot{\boldsymbol{u}}_{\boldsymbol{k}})^T$. The matrix $D(\boldsymbol{k})$ is Hermitian and positive definite, which guarantees that the system is mechanically stable.

Because the Hermitian matrix $D(\boldsymbol{k})$ is positive definite, we can introduce a Hermitian matrix $Q(\boldsymbol{k})$ with $D(\boldsymbol{k}) = Q^2(\boldsymbol{k})$ (for more details, see Appendix A). Thus, the equation of motion (2) is rewritten as [6,8]

$$i\partial_t \boldsymbol{\psi}(t) = H\boldsymbol{\psi}(t), \tag{3a}$$

$$H = \begin{pmatrix} 0 & Q(\boldsymbol{k}) \\ Q(\boldsymbol{k}) & i\Gamma_0(\boldsymbol{k}) \end{pmatrix}_{\rho}, \tag{3b}$$

with

$$\boldsymbol{\psi}(t) = \begin{pmatrix} Q(\boldsymbol{k}) & 0 \\ 0 & i\mathbb{1} \end{pmatrix}_{\rho} \boldsymbol{\phi}(t). \tag{3c}$$

The matrices H and M in Eq. (2a) give the same eigenvalues (i.e., the same frequency). Therefore, the dynamics of the system is described by the matrix H which is Hermitian in the absence of dissipation. Because Eq. (3) is mathematically identical to the Schrödinger equation, we refer to the matrix H as Hamiltonian in the following. When $i\Gamma_0(\boldsymbol{k})$ is a Hermitian, the system conserves the energy. Otherwise, the system is dissipative.

B. Emergent symmetry

Remarkably, mechanical systems possess extended chiral symmetry as an emergent property; in contrast to other platforms of non-Hermitian physics (e.g., quantum systems or

photonic crystals), the Hamiltonian H describing mechanical systems preserves extended chiral symmetry (4) regardless of its details. Furthermore, the system preserves CP symmetry (6), provided that the inversion symmetry is present. In the following, we see the details.

(i) *Emergent symmetry*. Any system, whose matrix $\Gamma_0(\boldsymbol{k})$ purely describes loss of energy, possesses the extended chiral symmetry as an emergent property

$$\rho_3 H^{\dagger}(\boldsymbol{k})\rho_3 = -H(\boldsymbol{k}), \tag{4}$$

where ρ's are Pauli matrices. Mathematically, the above emergent symmetry is preserved if $i\Gamma_0(\boldsymbol{k})$ is anti-Hermitian. Introducing the Coriolis force or the Lorentz force breaks the extended chiral symmetry.

(ii) *CP symmetry*. When the system is inversion symmetric, the CP symmetry is preserved. To see this, we first mention particle-hole symmetry of mechanical systems. Particle-hole symmetry is preserved for any D and Γ_0 rewritten as real matrices in the real space. Namely, when the matrices satisfy $D^*(\boldsymbol{k}) = D(-\boldsymbol{k})$ and $\Gamma_0^*(\boldsymbol{k}) = \Gamma_0(-\boldsymbol{k})$, the system preserves the particle-hole symmetry

$$\rho_3 H^*(\boldsymbol{k})\rho_3 = -H(-\boldsymbol{k}). \tag{5}$$

Thus, if the system is inversion symmetric [i.e, $U_I D(\boldsymbol{k})U_I = D(-\boldsymbol{k})$ and $U_I \Gamma_0(\boldsymbol{k})U_I = \Gamma_0(-\boldsymbol{k})$ with $U_I^2 = \mathbb{1}$ hold], the Hamiltonian preserves the CP symmetry

$$U_{CP}H^*(\boldsymbol{k})U_{CP}^{\dagger} = -H(\boldsymbol{k}), \tag{6}$$

with $U_{CP} = U_I \otimes \rho_3$. CP symmetry may exist even when the Coriolis force is present. However, to preserve the CP symmetry, the system needs to be inversion symmetric, which requires fine tuning. We note that the matrix $Q(\boldsymbol{k})$ inherits symmetry of the matrix $D(\boldsymbol{k})$ (for more details see Appendix A).

We note that particle-hole symmetry itself is another type of emergent symmetry [8]. However, it requires momentum flipping and thus irrelevant for symmetry-protected non-Hermitian degeneracies.

C. Symmetry-protected non-Hermitian degeneracies with extended chiral symmetry

Here, we show that the extended chiral symmetry (4) results in symmetry-protected non-Hermitian topological degeneracies [48] by analyzing the Hamiltonian around a band-touching point. The topological characterization of these degeneracies is discussed in Sec. III B.

First, we note that in the presence of the extended chiral symmetry, the energy eigenvalues form a pair $(E, -E^*)$ or take pure imaginary values ($E \in i\mathbb{R}$) (see Appendix B). This fact indicates that each pair $(E, -E^*)$ cannot split without going through a band touching (i.e., band touching both for real and imaginary parts).

Let us consider a one-dimensional line in the BZ where a pair of bands splits via a band-touching point. As we see below, the Hamiltonian is defective at this band-touching point. Around but not at the band-touching point, we first project the Hilbert space to the space spanned by the pair of bands. Then, the Hamiltonian and the operator of extended chiral symmetry are reduced into 2×2 matrices. Here, the

chiral operator is written as $U_\Gamma = \boldsymbol{n} \cdot \boldsymbol{\sigma}$ [52] with a unit vector $\boldsymbol{n} \in \mathbb{R}^3$. Therefore, without loss of generality, the Hamiltonian and the operator of extended chiral symmetry are written as

$$H = id_0\sigma_0 + (\boldsymbol{b} + i\boldsymbol{d}) \cdot \boldsymbol{\sigma}, \tag{7a}$$

$$U_\Gamma = \sigma_3, \tag{7b}$$

with $\boldsymbol{b} = (b_1, b_2, 0)$ and $\boldsymbol{d} = (0, 0, d_3)$. The eigenvalues of the Hamiltonian H are written as

$$E = id_0 \pm \sqrt{b^2 - d^2}. \tag{7c}$$

Therefore, at the band-touching point satisfying $b = d$, the Hamiltonian is written as $H = \begin{pmatrix} id_0 & b \\ 0 & id_0 \end{pmatrix}$ with a proper choice of the basis. This result indicates that the Hamiltonian is defective [53] (i.e., it is not diagonalizable).

We note that CP symmetry also results in symmetry-protected non-Hermitian degeneracies, which can be seen in a similar way as the above case (see Appendix C).

III. SPERS FOR A MECHANICAL GRAPHENE WITH FRICTION

We demonstrate the emergence of the SPERs for a mechanical graphene with friction (Fig. 1).

A. Model

We first consider only potential forces. After that the Coriolis force and friction are introduced. We consider that the spring mass forms the honeycomb lattice whose unit cell is illustrated with a red dashed box in Fig. 1. In this figure, primitive translation vectors $\boldsymbol{a}_1$ and $\boldsymbol{a}_2$ are shown with blue arrows. We also suppose that the mass points are trapped in harmonic potentials arising from gravity, which can be realized by introducing dents of the floor. When the displacement
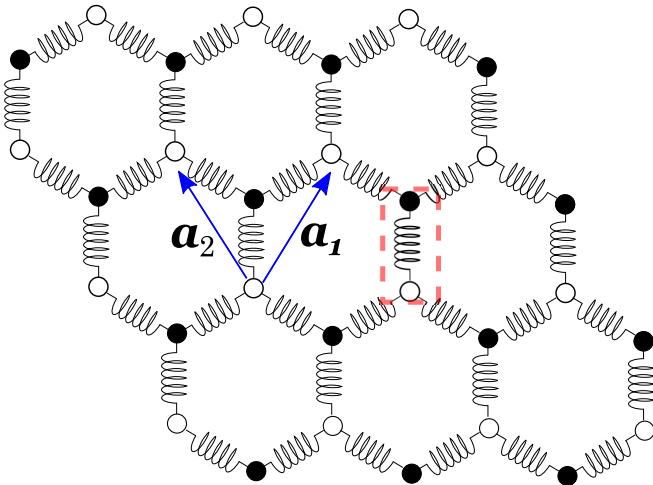

FIG. 1. Sketch of the mechanical graphene where mass points are connected by springs. The system is composed of A and B sublattices represented with white and black circles. The unit cell is enclosed with the red dashed box. $\boldsymbol{a}_1$ and $\boldsymbol{a}_2$ are the primitive translation vectors. We note that the system is horizontal.

is sufficiently smaller than the lattice constant, the Lagrangian is represented as the following quadratic form:

$$\mathcal{L} = \frac{m}{2} \sum_{\boldsymbol{k},\mu,\alpha} \dot{u}^\mu_{\boldsymbol{k}\alpha} \cdot \dot{u}^\mu_{-\boldsymbol{k}\alpha} - \frac{1}{2} \sum_{\boldsymbol{k}} D^{\mu\nu}_{\alpha\beta}(\boldsymbol{k}) u^\mu_{\boldsymbol{k},\alpha} u^\nu_{-\boldsymbol{k},\beta}, \tag{8a}$$

with $D^{\mu\nu}_{\alpha\beta}(\boldsymbol{k}) = D_{\mu\alpha;\nu\beta}(\boldsymbol{k})$ and

$$D(\boldsymbol{k}) = 3\kappa\left(1 - \frac{\eta}{2}\right)\mathbb{1} + \begin{pmatrix} \kappa^0_A & D_{AB}(\boldsymbol{k}) \\ D^\dagger_{AB}(\boldsymbol{k}) & \kappa^0_B \end{pmatrix}, \tag{8b}$$

$$D_{AB}(\boldsymbol{k}) = \kappa(\gamma_3 + \gamma_1 e^{-i\boldsymbol{k}\cdot\boldsymbol{a}_1} + \gamma_2 e^{-i\boldsymbol{k}\cdot\boldsymbol{a}_2}), \tag{8c}$$

$$\gamma_1 := (1 - \eta)\begin{pmatrix} 1 & 0 \\ 0 & 1 \end{pmatrix} + \eta\begin{pmatrix} \frac{3}{4} & \frac{\sqrt{3}}{4} \\ \frac{\sqrt{3}}{4} & \frac{1}{4} \end{pmatrix}, \tag{8d}$$

$$\gamma_2 := (1 - \eta)\begin{pmatrix} 1 & 0 \\ 0 & 1 \end{pmatrix} + \eta\begin{pmatrix} \frac{3}{4} & -\frac{\sqrt{3}}{4} \\ -\frac{\sqrt{3}}{4} & \frac{1}{4} \end{pmatrix}, \tag{8e}$$

$$\gamma_3 := (1 - \eta)\begin{pmatrix} 1 & 0 \\ 0 & 1 \end{pmatrix} + \eta\begin{pmatrix} 0 & 0 \\ 0 & 1 \end{pmatrix}. \tag{8f}$$

Here, m denotes the mass and κ describes the potential force of springs. κ^0_α denotes the strength of the potential force arising from the gravity for sublattice α ($\alpha = A, B$). $u^\mu_{\boldsymbol{k}\alpha}$ denotes the Fourier transformed displacement of the mass point at α sublattice. The $\mu(= x, y)$ denotes the μ component. Prestress in the spring is controlled by $\eta := l_0/R$ [7] where l_0 denotes natural length of the spring and R denotes lattice constant ($R = 1$).

Taking variational derivative of the Lagrangian, we obtain the equation of motion

$$\ddot{u}^\mu_{\boldsymbol{k}\alpha} = -D^{\mu\nu}_{\alpha\beta}(\boldsymbol{k})u^\nu_{\boldsymbol{k}\beta}. \tag{9}$$

Now, let us introduce the frictional force and the Coriolis force which are proportional to velocity, the equation of motion is written as

$$\ddot{u}^\mu_{\boldsymbol{k}\alpha} = -D^{\mu\nu}_{\alpha\beta}(\boldsymbol{k})u^\nu_{\boldsymbol{k}\beta} + \Gamma^{\mu\nu}_{0\alpha\beta}(\boldsymbol{k})\dot{u}^\nu_{\boldsymbol{k}\beta}, \tag{10a}$$

$$\Gamma^{\mu\nu}_{0\alpha\beta} = -b_\alpha\delta^{\mu\nu}\delta_{\alpha\beta} + \Omega_0\epsilon^{\mu\nu}\delta_{\alpha\beta}, \tag{10b}$$

with $\Omega_0 \in \mathbb{R}$ and $b_\alpha \geqslant 0$. Here, summation over repeating indices is assumed. $\epsilon^{\mu\nu}$ is an antisymmetric matrix with $\epsilon^{xy} = 1$. The term proportional to b_α describes the frictional force, and the term proportional to Ω_0 describes the Coriolis force (i.e., Ω_0 denotes the angular velocity).

We note that Eqs. (1) and (10) describing the above system are rewritten in the form of Eq. (3) with $\boldsymbol{\phi} = (\boldsymbol{u}_{\boldsymbol{k}}, \dot{\boldsymbol{u}}_{\boldsymbol{k}})^T$ and $\boldsymbol{u}_{\boldsymbol{k}} = (u^x_{\boldsymbol{k}A} \quad u^y_{\boldsymbol{k}A} \quad u^x_{\boldsymbol{k}B} \quad u^y_{\boldsymbol{k}B})^T$.

Here, we briefly summarize the symmetry. When the Coriolis force is absent, the system preserves extended chiral symmetry (4) regardless of the other details of the system. Aside from the extended chiral symmetry, CP symmetry (6) with $U_{CP} = \mathbb{1} \otimes s_1 \otimes \rho_3$ is preserved because our system is inversion symmetric. Here, s_i ($i = 1, 2, 3$) denotes the Pauli matrix acting on the sublattice degrees of freedom. Due to the above symmetry, SPERs may emerge in the mechanical graphene.
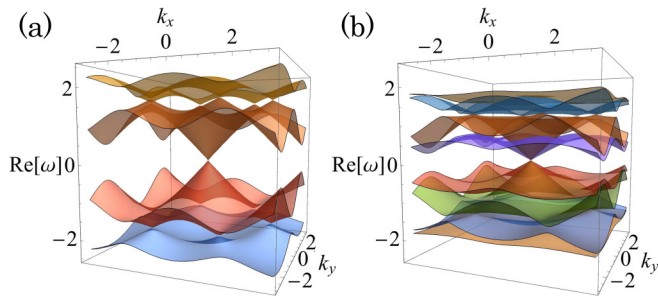
FIG. 2. (a) [(b)] Energy dispersion $\omega(\boldsymbol{k})$ of the mechanical graphene for $(b, \eta) = (0, 0)$ and [$(b, \eta) = (0, 0.8)$].

B. Numerical demonstration

We demonstrate that the mechanical graphene hosts SPERs. Specifically, after the results of the conservative system, we show the presence of SPERs with the extended chiral symmetry (4) for the system with friction (Sec. III B 2). In Sec. III B 3, we show that SPERs survive even in the absence of the extended chiral symmetry. This is because the system preserves CP symmetry (6). In Sec. III B 4, we see that breaking both of the extended chiral symmetry and CP symmetry changes the SPERs to exceptional points.

In the following, we discuss the data for $m = \kappa = 1$.

1. System without friction

Let us start with the case of $b_A = b_B = 0$ where the system is not dissipative. By diagonalizing the matrix $M(\boldsymbol{k})$, we obtain the band structure for $\eta = 0$ which is plotted in Fig. 2(a). In this case, the longitudinal and transverse waves are decoupled, which results in twofold degeneracy of each band as shown in Fig. 2(a). Increasing η lifts the degeneracy [see Fig. 2(b)]. For both cases of $\eta = 0$ and 0.8, one can observe the following two behaviors: (i) the linear dispersion is observed around the Γ point, which corresponds to the Nambu-Goldstone modes; (ii) the real part of the energy eigenvalue is symmetric for $\text{Re}[\omega] = 0$, which arises from extended chiral symmetry and CP symmetry [see Eqs. (4) and (6)].

2. System with friction

Now, we move on to the system with friction by setting $b = 0.5$. In this case, the eigenvalues ω take complex values. The real and the imaginary parts of the energy eigenvalues for $\eta = 0.8$ are plotted in Figs. 3(a) and 3(b), respectively. Because of the extended chiral symmetry, eigenvalues (ω's) form a pair ($\omega, -\omega^*$) or take pure imaginary $\omega \in i\mathbb{R}$, indicating that each pair cannot split without showing a band touching (see Sec. II C). Correspondingly, energy eigenvalues satisfy $\text{Im}[\omega] = -b/2$ in the region where $\text{Re}[\omega] \neq 0$. We note that the Hamiltonian is written as Eq. (E2) up to the term $(-ib/2)\mathbb{1}$.

As discussed in Sec. II C, the Hamiltonian becomes defective (i.e., it is not diagonalizable) at the ring of band-touching points. This can be seen in Fig. 3(c). This figure shows points in the BZ where the determinant of the matrix $U(\boldsymbol{k})$ becomes zero. Here, each column of the matrix $U(\boldsymbol{k})$, which is a square matrix of order $\dim M$, corresponds to the eigenvectors
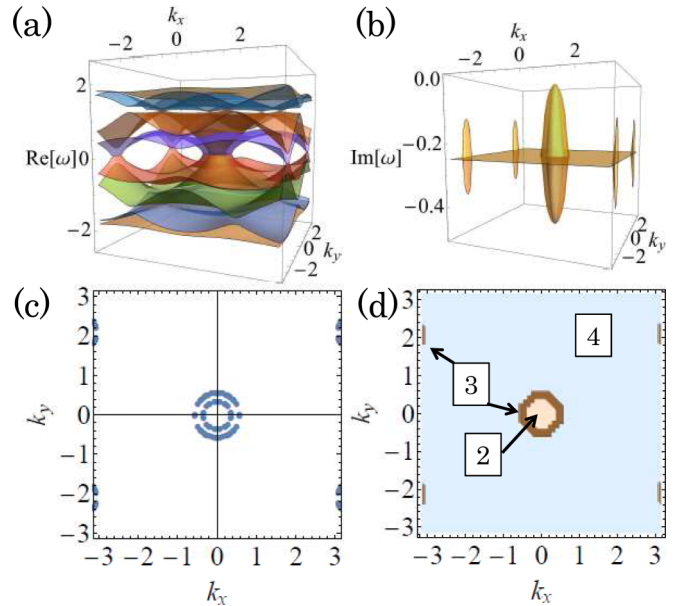

FIG. 3. Numerical results of the mechanical graphene with friction. (a) [(b)] The real part (imaginary part) of the eigenvalues $\omega(\boldsymbol{k})$. (c) Momentum points $\boldsymbol{k}_0$ satisfying $|\det U(\boldsymbol{k}_0)| < 0.005$. (d) The zeroth Chern number $N_{0\text{Ch}}$ [i.e., the number of occupied bands for $-iH'\rho_3$ with $H' = H - (\text{tr}H/\dim H)\mathbb{1}$] at each point of the BZ. For computation of $N_{0\text{Ch}}$, we have used Eq. (11). The data are obtained for $\Omega = \kappa_A = \kappa_B = 0$ and $(b, \eta) = (0.5, 0.8)$ with $b_A = b_b = b = 0.5$. We note that the imaginary part of eigenvalues takes a distinct value except for the case of $\text{Im}[\omega] = -b/2$.

of $M(\boldsymbol{k})$. Therefore, on the points plotted in Fig. 3(c), the Hamiltonian becomes defective. We note that for some modes, the damping rate inside of the SPER becomes smaller than the one outside of the SPER [see Fig. 3(b)], which holds for generic systems with homogeneous friction [54]. Therefore, the emergence of SPER results in the following dynamical behavior which may be observed in experiments. A region emerges in the BZ for which the displacement damps slowly compared to the ones for the other region. The modes on the exceptional rings show critical damping.

Here, we address the characterization of the exceptional points. As pointed out in Ref. [48], SPERs are characterized with the zeroth Chern number (the definition is in Appendix E). This fact is consistent with $\mathbb{Z}$ classification for class BDI with $\delta = 1$ (see Sec. IV). Figure 3(d) shows that the SPERs emerge at the boundary separating two domains with distinct values of $N_{0\text{Ch}}$, which characterizes the SPERs. Interestingly, when the frictional force is homogeneous, the zeroth Chern number $N_{0\text{Ch}}$ can be simplified as

$$N_{0\text{Ch}}(\boldsymbol{k}) = \sum_{n=1,\ldots,\dim H} \Theta_>[2\omega_{0n}(\boldsymbol{k}) - b] \qquad (11)$$

when the frictional force is homogeneous. $\Theta_>(x)$ takes 1, $\frac{1}{2}$, and 0 for $x > 0$, $x = 0$, and $x < 0$, respectively. ω_{0n} ($n = 1, \ldots, \dim H$) is the energy eigenvalue of the system without friction. The details of the derivation are summarized in Appendix E. Remarkably, the right-hand side of Eq. (11) is composed only with experimental observables, indicating that the $N_{0\text{Ch}}$ is measurable in experiments.
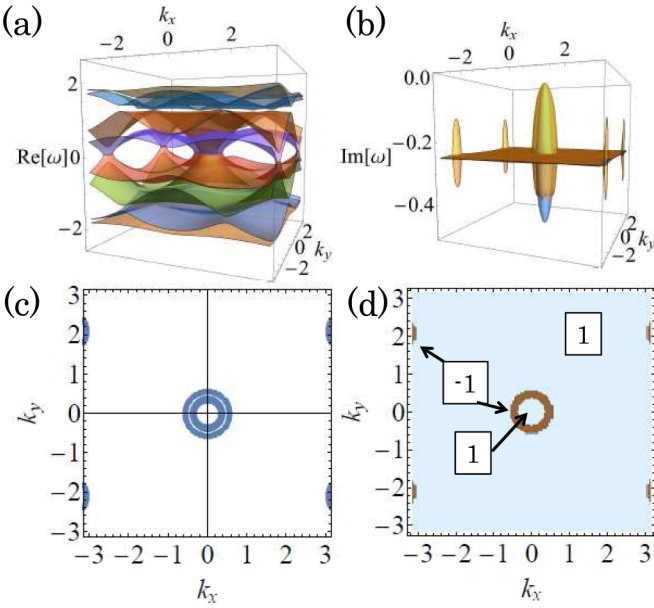
FIG. 4. Numerical results of the rotating mechanical graphene with homogeneous friction. (a) [(b)] The real part (imaginary part) of the eigenvalues $\omega(\boldsymbol{k})$. (c) Momentum points $\boldsymbol{k}_0$ satisfying $|\det U(\boldsymbol{k}_0)| < 0.005$. (d) The $\mathbb{Z}_2$ invariant (12) for each point of the BZ. The data are obtained for $\kappa_A = \kappa_B = 0$ and $(b, \Omega_0, \eta) = (0.5, 0.05, 0.8)$ with $b_A = b_b = b = 0.5$.

We consider that the zeroth Chern number and the presence of the region where the modes damp slowly are experimental signals of SPERs.

3. Rotating system with homogeneous friction

As seen in Sec. II C, the robustness of the exceptional rings in this two-dimensional system arise from the extended chiral symmetry (4). Here, we see that the SPERs in the mechanical graphene can survive even in the absence of the extended chiral symmetry. In order to see this, we here analyze effects of the symmetry breaking. First, we analyze the system by introducing the Coriolis force which breaks the extended chiral symmetry. Figures 4(a) and 4(b) show the real and the imaginary parts of the eigenvalues for the parameter set $(b_A, b_B, \Omega_0, \kappa_B, \eta) = (0.5, 0.5, 0.05, 0, 0.8)$, respectively. These figures show that band-touching points form a ring. Figure 4(c) elucidates the points where the matrix $M(\boldsymbol{k})$ becomes defective. These figures indicate that the SPERs survive even in the absence of the extended chiral symmetry. In this case, the SPERs are protected by CP symmetry (6) (see Appendix C).

Classification results obtained in Sec. IV elucidate that the SPERs can be characterized by the $\mathbb{Z}_2$ invariant. The $\mathbb{Z}_2$ invariant of the zero-dimensional systems is given by [43]

$$s(\boldsymbol{k}) = \mathrm{sgn}[\det i H'(\boldsymbol{k})], \tag{12}$$

with $H' = H - (\mathrm{tr}H/\dim H)\mathbb{1}$. Here, $\mathrm{sgn}(x)$ take 1 and -1 for $x > 0$ and $x < 0$. In Fig. 4(d), one can see that the $\mathbb{Z}_2$ invariant characterizes the SPERs.
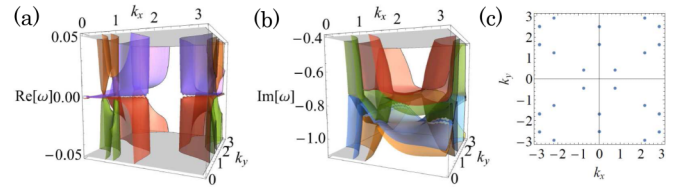

FIG. 5. Numerical results of the rotating mechanical graphene with inhomogeneous friction and the harmonic potentials. The data are obtained for $(b_A, \Omega_0, \kappa_B, \eta) = (2, 0.05, 0.05, 0.8)$ and $b_B = \kappa_A = 0$. (a) [(b)] The real part (imaginary part) of the eigenvalues $\omega(\boldsymbol{k})$. (c) Momentum points $\boldsymbol{k}_0$ satisfying $|\det U(\boldsymbol{k}_0)| < 0.005$.

4. Rotating system with inhomogeneous friction and the harmonic potentials

Further breaking CP symmetry changes the SPER to the exceptional points. Figure 5 shows data for the parameter set $(b_A, b_B, \Omega_0, \kappa_A, \kappa_B, \eta) = (2, 0, 0.05, 0, 0.05, 0.8)$. Figures 5(a) and 5(b) show that the band touching occurs at points rather than rings [55]. Correspondingly, the points, where the determinant of the matrix U approaches to zero, does not form rings [see Fig. 5(c)]. The above results indicate that exceptional points appear for mechanical systems when the systems have neither the extended chiral symmetry nor CP symmetry.

With breaking CP symmetry but preserving extended chiral symmetry, we can observe the SPERs with extended chiral symmetry.

IV. CLASSIFICATION OF THE NON-HERMITIAN DEGENERACIES IN MECHANICAL SYSTEMS

So far, we have observed the existence of SPERs in the mechanical graphene with extended chiral symmetry (4), which is an emergent property of mechanical systems. The mechanism of symmetry protection has been discussed in Sec. II C.

In this section, we address classification of topological non-Hermitian degeneracies, which allows us to discuss the symmetry protection in a more systematic way. The classification results also predict topological non-Hermitian degeneracies for other cases of symmetry and dimensions, which is summarized in Sec. IV C 1.

The above issue has recently been addressed for generic non-Hermitian matrices [56]. However, we would like to stress that the special characteristics, such as the emergent symmetry, need to be taken into account for systematic understanding of non-Hermitian degeneracies in mechanical systems, which is supported by the numerical results in Sec. III B.

A. Relevant symmetry

In Sec. II B, we have seen that mechanical systems may preserve extended chiral symmetry (4) and the CP symmetry (6). Therefore, we address the topological classification for the following symmetry constraints:

$$U_{TP}H^T(\boldsymbol{k})U_{TP}^\dagger = H(\boldsymbol{k}), \tag{13a}$$

$$U_{CP}H^*(\boldsymbol{k})U_{CP}^\dagger = -H(\boldsymbol{k}), \tag{13b}$$

$$U_\Gamma H^\dagger(\boldsymbol{k})U_\Gamma^\dagger = -H(\boldsymbol{k}). \tag{13c}$$

Equations (13b) and (13c) are generic forms of CP symmetry and extended chiral symmetry discussed in Sec. II B. The first condition is obtained by the product of Eqs. (13b) and (13c). As discussed in Sec. III B, the mechanical graphene may preserve the extended chiral symmetry and CP symmetry. Rotating the system violates Eq. (13c), and introducing inhomogeneity breaks Eq. (13b).

We note that for systems preserving CP symmetry with $(CP)^2 = -1$, additional CP symmetry $[CP' = U_{CP'}\mathcal{K}$ and $(CP')^2 = 1]$ should be taken into account. This is because particle-hole symmetry (5) is generically preserved for mechanical systems; Eq. (5) is satisfied for any D and Γ_0 rewritten as real matrices in the real space.

One may consider another type of CP symmetry $U_{CP}H^T(\mathbf{k})U_{CP}^{\dagger} = -H(\mathbf{k})$. However, this symmetry is incompatible with homogeneous friction (for more details see Appendix G). Therefore, we only consider the symmetry shown in Eq. (13).

B. Brief description of classification scheme

In the following, we explain how to classify non-Hermitian topological degeneracies. This section describes technical details and the readers may skip them and directly proceed to Sec. IV C 1.

1. Band gap for non-Hermitian systems

As pointed out in Ref. [45], there are two ways to define the band gap for the non-Hermitian systems because the eigenvalues take complex values. The first one is the point gap [43] and the second one is the line gap [25]. The results obtained in Sec. III B indicate that adopting the point gap captures the SPERs and the symmetry-protected exceptional surfaces (SPESs), which we see below.

First, we define that a system is gapped when its Hamiltonian $H(\mathbf{k})$ satisfies $\det H(\mathbf{k}) \neq 0$. Second, consider two subsystems in the BZ whose point gap is finite. If the two Hamiltonians describing these subsystems are topologically distinct, then, the gap needs to close ($\det H = 0$) in a region separating the two subsystems, which corresponds to the non-Hermitian degeneracies.

2. Classification scheme

The classification of d_{EP}-dimensional non-Hermitian degeneracies (i.e., gapless nodes) in d spatial dimensions is accomplished by classifying ($\delta - 1$)-dimensional gapped Hamiltonian with $\delta = d - d_{\mathrm{EP}}$.

The strategy of the classification is mapping the non-Hermitian Hamiltonian to a Hermitian matrix whose classification is well established. Such mapping is accomplished by defining

$$\tilde{H}(\mathbf{k}) := \begin{pmatrix} 0 & H(\mathbf{k}) \\ H^{\dagger}(\mathbf{k}) & 0 \end{pmatrix}_{\chi}. \quad (14)$$

The condition $\det H = 0$ is equivalent to $\det \tilde{H} = 0$, indicating that the gap closing of the non-Hermitian Hamiltonian H can be captured with Hermitian Hamiltonian $\tilde{H}$.

Now, we discuss the symmetry constraints on $\tilde{H}$. The TP symmetry (13a) is rewritten as

$$\widetilde{TP}\tilde{H}(\mathbf{k})\widetilde{TP}^{-1} = \tilde{H}(\mathbf{k}), \quad (15a)$$

with $\widetilde{TP} = U_{TP} \otimes \chi_1 \mathcal{K}$. The CP symmetry (13a) is rewritten as

$$\widetilde{CP}\tilde{H}(\mathbf{k})\widetilde{CP}^{-1} = -\tilde{H}(\mathbf{k}), \quad (15b)$$

with $\widetilde{CP} = U_{CP} \otimes \chi_0 \mathcal{K}$. The extended chiral symmetry (13a) is rewritten as

$$\tilde{\Gamma}\tilde{H}(\mathbf{k})\tilde{\Gamma}^{-1} = -\tilde{H}(\mathbf{k}), \quad (15c)$$

with $\tilde{\Gamma} = U_{\Gamma} \otimes \chi_1$. Here, the operator $\mathcal{K}$ takes complex conjugation. χ's are the Pauli matrices acting on the extended Hilbert space. In addition to the above symmetry, the Hermitian Hamiltonian $\tilde{H}$ always preserves the chiral symmetry $\tilde{\Sigma} := \mathbb{1} \otimes \chi_3$.

Therefore, the topological classification of non-Hermitian degeneracies is reduced to the classification of the Hermitian Hamiltonian $\tilde{H}$ for tenfold way symmetry classes, which are called $\mathrm{AZ} + \mathcal{I}$ classes [57], in the presence of additional chiral symmetry $\Sigma = \mathbb{1} \otimes \chi_3$. The latter problem can be solved by approach based on the Clifford algebra. The detailed calculations are shown in Appendix H.

We remind that in the presence of CP symmetry with $(CP)^2 = -1$, there exists additional CP' symmetry with $(CP')^2 = 1$; CP' symmetry should be considered for symmetry classes CII, C, and CI. Thus, we need to carry out the classification for the corresponding Hermitian systems by taking into account the additional chiral symmetry Σ and CP' symmetry, which is discussed in Appendix H 3.

C. Classification results

1. Overview

Tables I and II summarize the classification results of d_{EP}-dimensional non-Hermitian topological degeneracies in the d-dimensional BZ, specifying the relevant symmetry of the mechanical systems. This classification results elucidate the presence/absence of a topological invariant for the ($\delta - 1$)-dimensional subspace of the BZ with $\delta := d - d_{\mathrm{EP}}$; e.g., zero-dimensional topological invariants of SPERs observed in Sec. III B correspond to the case of $\delta = 1$ [$(d, d_{\mathrm{EP}}) = (2, 1)$].

The mechanical graphene analyzed in Sec. III B belongs to classes A, BDI, or D. In particular, the results of classes BDI and D in Table I support the robustness of SPERs observed in Figs. 3 and 4. The mechanical graphene with homogeneous friction belongs to class BDI where the classification result is $\mathbb{Z}$ for $\delta = 1$. This fact indicates the presence of a zero-dimensional topological invariant (for more details, see Sec. IV C 2). Introducing the Coriolis force, the symmetry class changes to class D where the classification result is $\mathbb{Z}_2$ for $\delta = 1$, meaning the presence of a zero-dimensional $\mathbb{Z}_2$ invariant (for more details, see Sec. IV C 3).

Furthermore, Table I supports that a wide range of mechanical systems host SPERs in two dimensions. This can be seen by noticing the following facts: (i) the systems preserve extended chiral symmetry (4) as an emergent property when

TABLE I. Classification results for each case of codimension $\delta = d - d_{EP}$. Here, we consider d_{EP}-dimensional gapless node for d spatial dimensions. The "0" in the second, third, and fourth columns denotes that the corresponding symmetry is absent. The ± 1 in the second (the third) column represents the sign of $(TP)^2 = \pm 1$ [$(CP)^2 = \pm 1$], respectively. From sixth to ninth columns, the classification results are summarized where $\mathbb{Z}$ or $\mathbb{Z}_2$ means the presence of topological phases with the corresponding topological invariant. The "0" in these columns indicates the absence of topological phases. For symmetry classes CII, C, and CI, systems preserve CP' symmetry with $(CP')^2 = 1$ as well as CP symmetry with $(CP)^2 = -1$. This additional symmetry changes the classification results for these three symmetry classes. Thus, the results for CII and CI are shown in Table II. The classification results for d-dimensional gapped systems are obtained for $\delta = d + 1$.

	TP	CP	Γ	Homotopy	$\delta = 1$	2	3	4
A	0	0	0	$\pi_0(C_\delta)$	0	$\mathbb{Z}$	0	$\mathbb{Z}$
AIII	0	0	1	$\pi_0(C_{\delta-1})$	$\mathbb{Z}$	0	$\mathbb{Z}$	0
AI	1	0	0	$\pi_0(R_{\delta+6})$	0	$\mathbb{Z}$	$\mathbb{Z}_2$	$\mathbb{Z}_2$
BDI	1	1	1	$\pi_0(R_{\delta+7})$	$\mathbb{Z}$	$\mathbb{Z}_2$	$\mathbb{Z}_2$	0
D	0	1	0	$\pi_0(R_\delta)$	$\mathbb{Z}_2$	$\mathbb{Z}_2$	0	$\mathbb{Z}$
DIII	-1	1	1	$\pi_0(R_{\delta+1})$	$\mathbb{Z}_2$	0	$\mathbb{Z}$	0
AII	-1	0	0	$\pi_0(R_{\delta+2})$	0	$\mathbb{Z}$	0	0
CII	-1	-1	1					
C	0	-1	0	$\pi_0(C_\delta)$	0	$\mathbb{Z}$	0	$\mathbb{Z}$
CI	1	-1	1					

$\Gamma_0(\boldsymbol{k})$ describes only dissipative forces; (ii) these systems belong to class AIII if further symmetry is absent.

Table II summarizes classification results for systems preserving CP symmetry with $(CP)^2 = -1$. This table shows that classification results depend on commutation or anticommutation relation of the two operators, CP and CP', which is one of the special characteristics for mechanical systems. This table indicates the existence of symmetry-protected non-Hermitian degeneracies for class CII_+ which are characterized with a zero-dimensional topological invariant. We discuss this result by analyzing a 4×4 matrix in Sec. IV C 4.

In the following, we discuss the details.

2. SPERs in mechanical graphene

In Sec. III B 2, we have seen that the mechanical graphene for $\Omega_0 = 0$ and $b_A = b_B$ hosts SPERs with extended chiral

TABLE II. Classification results for symmetry classes CII and CI. In these cases, systems preserve CP' symmetry with $(CP')^2 = 1$ as well as CP symmetry with $(CP)^2 = -1$. $(CP)(CP') = (CP')(CP)$ holds for symmetry classes CII_+ and CI_+, while $(CP)(CP') = -(CP')(CP)$ holds for symmetry classes CII_- and CI_-.

	TP	CP	Γ	Homotopy	$\delta = 1$	2	3	4
CII_+	-1	-1	1	$\pi_0(C_{\delta-1})$	$\mathbb{Z}$	0	$\mathbb{Z}$	0
CI_+	1	-1	1	$\pi_0(C_{\delta-1})$	$\mathbb{Z}$	0	$\mathbb{Z}$	0
CII_-	-1	-1	1	$\pi_0(R_{\delta+2})$	0	$\mathbb{Z}$	0	0
CI_-	1	-1	1	$\pi_0(R_{\delta+6})$	0	$\mathbb{Z}$	$\mathbb{Z}_2$	$\mathbb{Z}_2$

symmetry. This fact can be seen from the classification results. The mechanical graphene preserves the CP symmetry [$(CP)^2 = 1$] as well as the extended chiral symmetry. Thus, the symmetry class is BDI where the classification result is $\mathbb{Z}$ for $\delta = 1$ (see Table I). Thus, the zeroth Chern number ($N_{0Ch} \in \mathbb{Z}$) can be defined at each point of the BZ, indicating the presence of SPERs and SPESs in two and three dimensions, respectively. Therefore, the mechanical graphene with homogeneous friction exemplifies $\mathbb{Z}$ classification of class BDI with $\delta = 1$, which is consistent with the result shown in Fig. 3(d).

Introducing inversion-symmetry-breaking terms changes the symmetry class from BDI to AIII. Table I indicates that the SPERs in the mechanical graphene survive even in the absence of inversion symmetry; the classification result of class AIII for $\delta = 1$ is $\mathbb{Z}$. This fact is consistent with our numerical simulation.

3. SPERs in rotating mechanical graphene

In Sec. III B 3 we have seen that the rotating mechanical system hosts SPERs with CP symmetry when the frictional force is homogeneous. This fact can be understood from the classification results. The rotating mechanical systems with inversion symmetry preserve CP symmetry. Thus, the rotating mechanical graphene belongs to class D where the classification result is $\mathbb{Z}_2$ for $\delta = 1$ (see Table I). Thus, the $\mathbb{Z}_2$ invariant (12) can be defined at each point of the BZ, indicating the presence of SPERs and SPESs in two and three dimensions, respectively. Therefore, the rotating mechanical system with homogeneous friction exemplifies the $\mathbb{Z}_2$ classification of class D [see also Fig. 4(d)].

Introducing inhomogeneity breaks CP symmetry and changes the symmetry class from D to A. Table I shows that the classification results of class A is 0 for $\delta = 1$ and $\mathbb{Z}$ for $\delta = 2$. This fact indicates that the system may have a one-dimensional $\mathbb{Z}$ invariant taking a nontrivial value, although there is no zero-dimensional topological invariant. This result explains the instability of SPERs against inhomogeneity for the rotating mechanical graphene; SPERs change into EPs due to inhomogeneity [see also Fig. 5(c)].

4. $\mathbb{Z}$ classification for CII_+ and $\delta = 1$

Tables I and II indicate the following facts. For class CII_+, there exist symmetry-protected non-Hermitian degeneracies characterized by a zero-dimensional $\mathbb{Z}$ invariant. These symmetry-protected non-Hermitian degeneracies are unstable against the perturbation breaking extended chiral symmetry (e.g., rotation) in contrast to the ones for class BDI. This is because the perturbation changes the symmetry from class CII_+ to class C where there is no topological invariant for $\delta = 1$.

In the following, we discuss the above results by analyzing a 4×4 matrix. Suppose that operators of TP and CP symmetry are given by

$$U_{TP} = i\tau_2 \rho_0, \tag{16a}$$

$$U_{CP} = i\tau_2 \rho_3, \tag{16b}$$

as well as these operators we assume that system preserves the CP' symmetry whose operator is given by

$$U_{CP'} = \tau_0 \rho_3. \tag{16c}$$

A 4×4 Hamiltonian satisfying the above symmetry is written as

$$H_{\mathrm{CII}_+} = id_{00}\tau_0\rho_0 + b_{01}\tau_0\rho_1 + b_{22}\tau_2\rho_2 + id_{03}\tau_0\rho_3. \tag{17}$$

For $b_{00} = b_{22} = 0$, the above Hamiltonian describes the one-dimensional subsystem of a mechanical square lattice ($k_x = k_y$) whose details are discussed in Appendix F. The eigenvalues of the Hamiltonian can be obtained as

$$E = id_{00} \pm \sqrt{b_{01}^2 + b_{02}^2 - d_{03}^2} \tag{18}$$

by noticing that it commutes with $U := U_{CP} U_{CP'}^* = \tau_2 \rho_0$. Therefore, satisfying only one condition results in the defective Hamiltonian (i.e., the nondiagonalizable Hamiltonian). This fact indicates the presence of exceptional points in the one-dimensional subsystem ($k_x = k_y$) of the mechanical square lattice, which corresponds to the case with $(d, d_{\mathrm{EP}}) = (1, 0)$.

Now, we add a perturbation breaking both of TP and extended chiral symmetry,

$$H' = b_{20}\tau_2\rho_0 + b_{23}\tau_2\rho_3 + id_{02}\rho_2\tau_0 + id_{21}\tau_2\rho_1. \tag{19}$$

The symmetry class of the resulting Hamiltonian ($H_{\mathrm{C}} := H_{\mathrm{CII}_+} + H'$) is class C. Because the system preserves CP and CP' symmetry, we can block diagonalize the Hamiltonian H_{C} with the matrix U [58]. Thus, the resulting eigenvalues of this model are written as

$$E_s = (sb_{20} + id_{00}) \pm \sqrt{b'^2 - d'^2 + 2is\boldsymbol{b}' \cdot \boldsymbol{d}'}, \tag{20}$$

with $\boldsymbol{b}' = (b_{01}, b_{22}, b_{23})$ and $\boldsymbol{b}' = (d_{21}, d_{02}, d_{03})$. Here, s takes ± 1, labeling each sector of U. Therefore, satisfying both of two conditions $b'^2 - d'^2 = 0$ and $\boldsymbol{b}' \cdot \boldsymbol{d}' = 0$ result in the defective Hamiltonian. This fact indicates that exceptional points in the subsystem ($k_x = k_y$) of the mechanical square lattice are unstable against rotation because rotating the system introduces the Coriolis force described by $b_{23}\tau_2\rho_3$ in Eq. (19).

V. SUMMARY

We have elucidated that mechanical systems host symmetry-protected non-Hermitian degeneracies (e.g., SPERs) with the extended chiral symmetry (4), which is an emergent property of mechanical systems. This fact indicates that mechanical systems are suited experimental platforms of symmetry-protected non-Hermitian degeneracies because fine tuning is not required in contrast to other experimental platforms (e.g., photonic systems). Specifically, we have demonstrated the emergence of the SPERs for the mechanical graphene with homogeneous friction. In this system, the zeroth Chern number, characterizing SPERs, can be obtained only from experimentally observable quantities; the coefficient of the fiction and the frequency for the case without dissipation. In addition, at any point inside of the SPERs, there exists a mode damping slowly compared to the one outside of the ring, which can be an experimental signal of SPERs.

Furthermore, we have carried out topological classification by taking into account the special characteristics of mechanical systems in order to systematically understand the interplay of non-Hermitian degeneracies and the emergent symmetry. The obtained results elucidate the presence of SPERs with CP symmetry for rotating mechanical graphene. The obtained results also predict symmetry-protected non-Hermitian degeneracies in two and three dimensions whose demonstration for specific mechanical systems is left as a future work.

APPENDIX A: SYMMETRY OF THE MATRIX $Q(\boldsymbol{k})$

We show that the matrix $Q(\boldsymbol{k})$, satisfying $D(\boldsymbol{k}) = Q^2(\boldsymbol{k})$, inherits symmetry of $D(\boldsymbol{k})$. First, we note that the matrix Q can be specifically obtained by diagonalizing D:

$$Q(\boldsymbol{k}) = U(\boldsymbol{k})\Lambda(\boldsymbol{k})^{1/2}U^\dagger(\boldsymbol{k}), \tag{A1a}$$

$$D(\boldsymbol{k}) = U(\boldsymbol{k})\Lambda(\boldsymbol{k})U^\dagger(\boldsymbol{k}), \tag{A1b}$$

where $U(\boldsymbol{k})$ is a unitary matrix. $\Lambda(\boldsymbol{k})$ is a diagonal matrix whose elements are eigenvalues of the positive-semidefinite matrix $D(\boldsymbol{k})$.

Now, we show that the following two relations hold.
For

$$U_I D(\boldsymbol{k}) U_I = D(-\boldsymbol{k}), \tag{A2a}$$

the matrix Q satisfies

$$U_I Q(\boldsymbol{k}) U_I = Q(-\boldsymbol{k}). \tag{A2b}$$

For

$$D^*(\boldsymbol{k}) = D(-\boldsymbol{k}), \tag{A3a}$$

the matrix Q satisfies

$$Q^*(\boldsymbol{k}) = Q(-\boldsymbol{k}). \tag{A3b}$$

First, we prove Eq. (A2b). As the condition (A2a) hold, we have

$$\begin{aligned} U_I Q(\boldsymbol{k}) U_I &= U_I [D^{1/2}(\boldsymbol{k})] U_I \\ &= [U_I D(\boldsymbol{k}) U_I]^{1/2} \\ &= [D(-\boldsymbol{k})]^{1/2} \\ &= Q(-\boldsymbol{k}), \end{aligned} \tag{A4}$$

which results in Eq. (A2b).

In a similar way, with Eq. (A3a), we have

$$\begin{aligned} Q^*(\boldsymbol{k}) &= [D^{1/2}(\boldsymbol{k})]^* \\ &= [D^*(\boldsymbol{k})]^{1/2} \\ &= [D(-\boldsymbol{k})]^{1/2} \\ &= Q^*(\boldsymbol{k}), \end{aligned} \tag{A5}$$

which results in Eq. (A3b).

APPENDIX B: EIGENVALUES OF HAMILTONIAN WITH EXTENDED CHIRAL SYMMETRY

Here, we show that in the presence of the extended chiral symmetry ($U_\Gamma H^\dagger U_\Gamma^\dagger = -H$), the energy eigenvalues form a pair ($E, -E^*$) or take pure imaginary values. Suppose that $|\phi_R^n\rangle$ and $|\phi_L^n\rangle$ are right and left eigenvectors of H:

$$H|\phi_R^n\rangle = E_n|\phi_R^n\rangle, \tag{B1a}$$

$$H^\dagger|\phi_L^n\rangle = E_n^*|\phi_L^n\rangle. \tag{B1b}$$

Then, we have

$$H^\dagger U_\Gamma|\phi_R^n\rangle = -U_\Gamma H|\phi_R^n\rangle = -E_n U_\Gamma|\phi_R^n\rangle. \tag{B2}$$

Comparing with Eq. (B1b), we see that the energy eigenvalues form a pair ($E, -E^*$) or are pure imaginary.

APPENDIX C: SYMMETRY-PROTECTED NON-HERMITIAN DEGENERACIES WITH *CP* SYMMETRY

1. Analysis of a 2 × 2 matrix around the band-touching point

Now, we elucidate that CP symmetry with $CP^2 = 1$ protects the SPERs in the two-dimensional BZ. (The following argument also holds for three-dimensional systems which host SPESs.)

First, we note that in the presence of CP symmetry (6), two eigenvalues of the Hamiltonian form a pair ($E, -E^*$) or become pure imaginary. This can be seen as follows. Consider the right eigenstate $|\phi_R^n\rangle$ of the Hamiltonian H with the eigenvalue E. Then, we obtain

$$HU|\phi_R^n\rangle^* = -UH^*|\phi_R^n\rangle^* = -E^*U|\phi_R^n\rangle^*, \tag{C1}$$

where we have used Eq. (6). The above fact indicates that each pair ($E, -E^*$) cannot split without going through a band touching.

Now, let us consider the case where two energy bands touch at a point in the BZ. Around the point the Hamiltonian can be represented as a 2 × 2 matrix which is generically given by

$$H_{2\times2}(\boldsymbol{k}) = \sum_{\alpha=0,...,3}(b_\alpha + id_\alpha)\sigma_\alpha. \tag{C2}$$

σ's are the Pauli matrices which act on the two states showing the band touching. In this two-dimensional Hilbert space, the CP operator is represented as $CP = \mathcal{K}$ ($CP = \sigma_2\mathcal{K}$) for $CP^2 = 1$ ($CP^2 = -1$), respectively. The derivation is shown in Appendix C 2. In the presence of CP symmetry with $CP = \mathcal{K}$, the generic Hamiltonian is written as

$$H_{2\times2}(\boldsymbol{k}) = \begin{pmatrix} i(d_0 + d_3) & id_1 - ib_2 \\ id_1 + ib_2 & i(d_0 - d_3) \end{pmatrix}. \tag{C3}$$

Diagonalizing the matrix yields

$$E_\pm(\boldsymbol{k}) = id_0 \pm \sqrt{b_2^2 - (d_1^2 + d_3^2)}, \tag{C4a}$$

indicating that the condition of the band touching is

$$b_2^2 = d_1^2 + d_3^2. \tag{C4b}$$

At the band-touching point, the Hamiltonian describing these two bands becomes defective because the Hamiltonian can be written as

$$H_{2\times2}(\boldsymbol{k}) = |b_2|\begin{pmatrix} 0 & 1 \\ 0 & 0 \end{pmatrix}. \tag{C5}$$

For $b^2 = d_1^2 + d_3^2 = 0$, the Hamiltonian becomes Hermitian and is diagonalizable. However, such condition cannot be satisfied without fine tuning. We note that the condition of the band touching (C4b) specifies a one-dimensional line in the BZ which corresponds to SPERs.

For $CP = \sigma_2\mathcal{K}$, the eigenvalue problem is reduced to the one for a Hermitian matrix because the CP symmetry results in

$$H_{2\times2}(\boldsymbol{k}) = id_0\sigma_0 + \sum_{\mu=1,2,3} b_\mu\sigma_\mu. \tag{C6}$$

2. Representation of the *CP* transformation

We show that the operator of CP symmetry is represented as

$$CP = \mathcal{K} \tag{C7}$$

for $CP^2 = 1$, and

$$CP = \sigma_2\mathcal{K} \tag{C8}$$

for $CP^2 = -1$. This can be seen as follows. A generic unitary matrix U_{CP} can be represented as

$$U_{CP} = e^{i\boldsymbol{b}\cdot\boldsymbol{\sigma}}, \tag{C9}$$

with $\boldsymbol{b} \in \mathbb{R}^3$ up to the global phase factor. Thus, we can see

$$U_{CP}U_{CP}^* = [\cos^2(b) + \sin^2(b)\hat{\boldsymbol{b}}\cdot\hat{\boldsymbol{b}}']$$
$$+ i\left[\sin^2 b(\boldsymbol{b}\times\boldsymbol{b}') + \tfrac{1}{2}\sin(2b)(\hat{\boldsymbol{b}}-\hat{\boldsymbol{b}}')\right]\cdot\boldsymbol{\sigma}, \tag{C10}$$

with $\boldsymbol{b} := (b_1, b_2, b_3)$ and $\boldsymbol{b}' := (b_1, -b_2, b_3)$. $\hat{\boldsymbol{b}}$ ($\hat{\boldsymbol{b}}'$) is a unit vector proportional to $\hat{\boldsymbol{b}}$ ($\hat{\boldsymbol{b}}'$) respectively.

Because $U_{CP}U_{CP}^*$ is proportional to the identity operator, we see that one of the following conditions are satisfied: (i) $b = n\pi$ with $n = 0, 1, 2, \ldots$, (ii) $\boldsymbol{b} = (b_1, 0, b_3)^T$, and (iii) $\boldsymbol{b} = (0, b_2, 0)^T$. For cases (i) and (ii), we have $U_{CP} = \sigma_0$. For case (iii), we have $U_{CP} = \sigma_2$.

For case (ii), we note that $\boldsymbol{b}\cdot\boldsymbol{\sigma}$ with $\boldsymbol{b} = (b_1, 0, b_3)^T$ is a real-symmetric matrix which can be diagonalized with an orthogonal matrix. Thus, without loss of generality, we have $U_{CP} = \sigma_0 = \cos(b)\sigma_0 + i\sin(b)\sigma_3$ which is reduced to $U_{CP} = \sigma_0$ by a proper choice of the gauge.

APPENDIX D: DETAILS OF THE MECHANICAL GRAPHENE

Here, we derive Eq. (8). We suppose that the dissipation and the internal force are absent and that the spring mass forms the honeycomb lattice (Fig. 1).

As a first step, we focus on the two mass points of this spring-mass system [Fig. 6(a)]. In this case, the potential energy arising from the spring is described as

$$U_s = \frac{\kappa}{2}\left(\sqrt{R_0^2 + \delta\boldsymbol{x}} - l_0\right), \tag{D1}$$
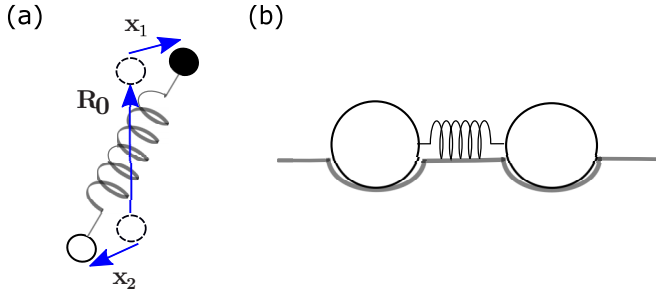
FIG. 6. Sketch of the system. (a) Two mass points connected with a spring. (b) Mass points trapped by dents of the floor.

where l_0 denotes natural length of the spring, and κ denotes a spring constant. Two-dimensional vectors are shown in Fig. 6(a); $\boldsymbol{R}_0$ connects two lattice points: $\delta\boldsymbol{x} := \boldsymbol{x}_1 - \boldsymbol{x}_2$ where $\boldsymbol{x}_i$ ($i = 1, 2$) describes the displacement of mass points. Supposing that $\delta x \ll R_0$, the potential energy can be expanded as

$$U_s = \frac{\kappa}{2}\left[(R_0 - l_0)^2 + 2(1 - \eta^{-1})\boldsymbol{R} \cdot \delta\boldsymbol{x} + \delta x_\mu \gamma_{\boldsymbol{R}_0}^{\mu\nu} \delta x_\nu\right],$$
(D2)

with $\mu = x, y$, $\hat{\boldsymbol{R}}_0 = \boldsymbol{R}_0/R_0$, and $\gamma_{\boldsymbol{R}_0}^{\mu\nu} = (1 - \eta)\delta^{\mu\nu} + \eta\hat{R}_0^\mu \hat{R}_0^\nu$.

Therefore, the Lagrangian of the mass points with mass m is given by

$$\mathcal{L} = T - U_1 - U_2,$$
(D3a)

$$T = \frac{m}{2}\sum_i \dot{\boldsymbol{x}}_i^2,$$
(D3b)

$$U_1 = \sum_i \frac{\kappa_i^0}{2}\boldsymbol{x}_i^2,$$
(D3c)

$$U_2 = \frac{\kappa}{2}\sum_{\langle ij\rangle}\left[(R_{ij} - l_0)^2 + 2(1 - \eta^{-1})\boldsymbol{R}_{ij} \cdot (\boldsymbol{x}_i - \boldsymbol{x}_j)\right.$$
$$\left. + (x_{i\mu} - x_{j\mu})\gamma_{\boldsymbol{R}_{ij}}^{\mu\nu}(x_{i\nu} - x_{j\nu})\right].$$
(D3d)

Here, we assume that the mass points are trapped on dents of the floor [Fig. 6(b)], which induces the potential term U_1. κ_i^0 describes strength of the harmonic potential arising from the dents of the floor. $\kappa_i^0 = \kappa_\alpha^0$ when the site i belongs to sublattice α. U_2 describes the potential energy arising from the springs. i and j label mass points. R_i denotes the equilibrium position of mass point i. $\boldsymbol{R}_{ij} := \boldsymbol{R}_i - \boldsymbol{R}_j$. The second term of Eq. (D3d) is zero as long as the equilibrium is achieved for $\boldsymbol{x}_i = 0$. Thus, we omit it.

Applying Fourier transformation,

$$\boldsymbol{u}_{\boldsymbol{k}\alpha}(t) = \frac{1}{\sqrt{N}}\sum_{i\in\alpha}e^{i\boldsymbol{k}\cdot\tilde{\boldsymbol{R}}_i}\boldsymbol{x}_{\tilde{R}_i\alpha}(t),$$
(D4)

the Lagrangian is rewritten as

$$\mathcal{L} = \frac{m}{2}\sum_{\boldsymbol{k},\mu,\alpha}\dot{u}_{\boldsymbol{k}\alpha}^\mu \cdot \dot{u}_{-\boldsymbol{k}\alpha}^\mu - \frac{1}{2}\sum_{\boldsymbol{k}}D_{\alpha\beta}^{\mu\nu}(\boldsymbol{k})u_{\boldsymbol{k},\alpha}^\mu u_{-\boldsymbol{k},\beta}^\nu,$$
(D5a)

with $D_{\alpha\beta}^{\mu\nu}(\boldsymbol{k}) = D_{\mu\alpha;\nu\beta}(\boldsymbol{k})$ and

$$D_{\mu\alpha;\nu\beta}(\boldsymbol{k}) = 3\kappa\left(1 - \frac{\eta}{2}\right)\mathbb{1} + \begin{pmatrix} \kappa_A^0 & D_{AB}(\boldsymbol{k}) \\ D_{AB}^\dagger(\boldsymbol{k}) & \kappa_B^0 \end{pmatrix},$$
(D5b)

$$D_{AB}^{\mu\nu}(\boldsymbol{k}) = -\kappa(\gamma_3 + \gamma_1 e^{-i\boldsymbol{k}\cdot\boldsymbol{a}_1} + \gamma_2 e^{-i\boldsymbol{k}\cdot\boldsymbol{a}_2}),$$
(D5c)

$$\gamma_1 := (1 - \eta)\begin{pmatrix} 1 & 0 \\ 0 & 1 \end{pmatrix} + \eta\begin{pmatrix} \frac{3}{4} & \frac{\sqrt{3}}{4} \\ \frac{\sqrt{3}}{4} & \frac{1}{4} \end{pmatrix},$$
(D5d)

$$\gamma_2 := (1 - \eta)\begin{pmatrix} 1 & 0 \\ 0 & 1 \end{pmatrix} + \eta\begin{pmatrix} \frac{3}{4} & -\frac{\sqrt{3}}{4} \\ -\frac{\sqrt{3}}{4} & \frac{1}{4} \end{pmatrix},$$
(D5e)

$$\gamma_3 := (1 - \eta)\begin{pmatrix} 1 & 0 \\ 0 & 1 \end{pmatrix} + \eta\begin{pmatrix} 0 & 0 \\ 0 & 1 \end{pmatrix}.$$
(D5f)

Here, $\boldsymbol{x}_{\tilde{R}_i\alpha}$ denotes the displacement of the mass point at $\alpha(= A, B)$ sublattice of the unit cell specified by $\tilde{\boldsymbol{R}}_i$. The above results correspond to Eq. (8).

APPENDIX E: SIMPLIFIED ZEROTH CHERN NUMBER FOR MECHANICAL SYSTEMS

First, we define the zeroth Chern number. Consider a traceless non-Hermitian Hamiltonian satisfying the extended chiral symmetry

$$U_\Gamma H^\dagger U_\Gamma^\dagger = -H,$$
(E1)

where U_Γ is a unitary matrix satisfying $U_\Gamma^2 = \mathbb{1}$. In this case, the zeroth Chern number counts the number of the occupied bands ($\epsilon_n < 0$) where ϵ_n with $n = 1, \ldots, \dim H$ denotes the eigenvalue of the Hermitian matrix $-iHU_\Gamma$.

The simplified form of the zeroth Chern number (11) can be obtained as follows. In the similar way as Sec. II A, for $\Gamma_0 = -b\mathbb{1}$ with $b > 0$, we can obtain the traceless Hamiltonian describing the mechanical system

$$H = \begin{pmatrix} i\frac{b}{2}\mathbb{1} & Q(\boldsymbol{k}) \\ Q(\boldsymbol{k}) & -i\frac{b}{2}\mathbb{1} \end{pmatrix},$$
(E2)

preserving the extended chiral symmetry with $\Gamma = \rho_3$. Here, the matrix Q is defined as $D = Q^2$ with the matrix D describing the potential force [see Eq. (A1)]. Namely, the eigenvalue of the matrix Q corresponds to the frequency of the oscillation $\omega_{0n}(\boldsymbol{k})$. Diagonalizing the matrix Q, the matrix $-iH\rho_3$ is rewritten as

$$-iH\rho_3 = \bigoplus_n \begin{pmatrix} \frac{b}{2} & i\omega_{0n} \\ -i\omega_{0n} & \frac{b}{2} \end{pmatrix}.$$
(E3)

Correspondingly, the eigenvalue ϵ_n is written as

$$\epsilon_n(\boldsymbol{k}) = \frac{b}{2} \pm \omega_{0n}(\boldsymbol{k}).$$
(E4)

Therefore, the zeroth Chern number is obtained as

$$N_{0\mathrm{Ch}}(\boldsymbol{k}) = \sum_{n=1,\ldots,\dim H}\Theta_>(2\omega_{0n}(\boldsymbol{k}) - b),$$
(E5)

where $\Theta_>(x)$ takes 1, $\frac{1}{2}$, and 0 for $x > 0$, $x = 0$, and $x < 0$, respectively. Notably, $N_{0\mathrm{Ch}}$ is obtained with the experimental observables for the mechanical system ω_{0n} and b.

APPENDIX F: MECHANICAL SQUARE LATTICE

In a similar way to Appendix D, we can obtain the Lagrangian of a spring-mass model forming a square lattice. The matrix $D(\boldsymbol{k})$ describing the potential force is written as

$$
\begin{aligned}
D(\boldsymbol{k}) = {}& 4\kappa\left(1 - \frac{\eta}{2}\right)\tau_0 - 2\kappa\Bigg[(1-\eta)[\cos(k_x) + \cos(k_y)]\tau_0 \\
& + \eta\cos(k_x)\begin{pmatrix} 1 & 0 \\ 0 & 0 \end{pmatrix}_\tau + \eta\cos(k_y)\begin{pmatrix} 0 & 0 \\ 0 & 1 \end{pmatrix}_\tau\Bigg] \\
= {}& 2\kappa\left(1 - \frac{\eta}{2}\right)\left[2 - 2\cos\left(\frac{k_x + k_y}{2}\right)\cos\left(\frac{k_x - k_y}{2}\right)\right]\tau_0 \\
& + 2\kappa\eta\sin\left(\frac{k_x + k_y}{2}\right)\sin\left(\frac{k_x - k_y}{2}\right)\tau_3.
\end{aligned}
\tag{F1}
$$

For $k_x - k_y = 0$, we can see that the term proportional to τ_3 vanishes. Therefore, for a system with a homogeneous frictional force, rewriting the equation of motion with Hamiltonian [see Eq. (3)], we can see that the obtained Hamiltonian corresponds to Eq. (17) with

$$
b_{00} = 0, \tag{F2}
$$

$$
b_{01} = \sqrt{4\kappa\left(1 - \frac{\eta}{2}\right)[1 - \cos(k_x)]}, \tag{F3}
$$

$$
b_{22} = 0, \tag{F4}
$$

where b_{03} in Eq. (17) describes the strength of the frictional force. Here, we have set the trap potential illustrated in Fig. 6(b) as zero.

APPENDIX G: ANOTHER TYPE OF *CP* SYMMETRY

Non-Hermiticity of the Hamiltonian results in two types of particle-hole symmetry [45]. One is given by Eq. (5) and the other is

$$
\rho_3 H^T(\boldsymbol{k})\rho_3 = -H(-\boldsymbol{k}). \tag{G1}
$$

However, we note that *CP* symmetry, defined as the product of particle-hole symmetry (G1) and inversion symmetry, is incompatible to mechanical systems with homogeneous friction, which is one of the simplest setups for non-Hermitian mechanical systems. When the Hamiltonian preserves the *CP* symmetry,

$$
U_{CP} H^T(\boldsymbol{k}) U_{CP}^\dagger = -H(\boldsymbol{k}), \tag{G2}
$$

with $U_{CP} = U_I \otimes \rho_3$ and $U_I^2 = \mathbb{1}$, we obtain

$$
U_I Q^T(\boldsymbol{k}) U_I = Q(\boldsymbol{k}), \tag{G3a}
$$

$$
U_I \Gamma_0^T(\boldsymbol{k}) U_I = -\Gamma_0(\boldsymbol{k}). \tag{G3b}
$$

For homogeneous friction $\Gamma_0 = -b\mathbb{1}$, the second equation yields $b = 0$, indicating that *CP* symmetry (G2) is incompatible to mechanical systems with homogeneous friction.

APPENDIX H: TENFOLD WAY CLASSIFICATION OF HERMITIAN HAMILTONIAN FOR AZ + $\mathcal{I}$ CLASSES WITH ADDITIONAL CHIRAL SYMMETRY

We address the topological classification of Hermitian topological insulators/superconductors in the presence or

TABLE III. Classification results for Hermitian systems of AZ+$\mathcal{I}$ symmetry classes with additional chiral symmetry. The "0" in the second, third, and fourth columns denotes that the corresponding symmetry is absent. The ± 1 in the second (the third) column represents the sign of $(TP)^2 = \pm 1$ [$(CP)^2 = \pm 1$], respectively. From sixth to thirteenth columns, the classification results are summarized where $\mathbb{Z}$ or $\mathbb{Z}_2$ means the presence of topological phases with the corresponding topological invariant. The "0" in these columns indicates the absence of topological phases.

	TP	CP	Γ	Homotopy	$d = 0$	1	2	3	4	5	6	7
A	0	0	0	$\pi_0(C_{d+1})$	0	$\mathbb{Z}$	0	$\mathbb{Z}$	0	$\mathbb{Z}$	0	$\mathbb{Z}$
AIII	0	0	1	$\pi_0(C_d)$	$\mathbb{Z}$	0	$\mathbb{Z}$	0	$\mathbb{Z}$	0	$\mathbb{Z}$	0
AI	1	0	0	$\pi_0(R_{d+7})$	0	$\mathbb{Z}$	$\mathbb{Z}_2$	$\mathbb{Z}_2$	0	$\mathbb{Z}$	0	0
BDI	1	1	1	$\pi_0(R_d)$	$\mathbb{Z}$	$\mathbb{Z}_2$	$\mathbb{Z}_2$	0	$\mathbb{Z}$	0	0	0
D	0	1	0	$\pi_0(R_{d+1})$	$\mathbb{Z}_2$	$\mathbb{Z}_2$	0	$\mathbb{Z}$	0	0	0	$\mathbb{Z}$
DIII	-1	1	1	$\pi_0(R_{d+2})$	$\mathbb{Z}_2$	0	$\mathbb{Z}$	0	0	0	$\mathbb{Z}$	$\mathbb{Z}_2$
AII	-1	0	0	$\pi_0(R_{d+3})$	0	$\mathbb{Z}$	0	0	0	$\mathbb{Z}$	$\mathbb{Z}_2$	$\mathbb{Z}_2$
CII	-1	-1	1	$\pi_0(R_{d+4})$	$\mathbb{Z}$	0	0	0	$\mathbb{Z}$	$\mathbb{Z}_2$	$\mathbb{Z}_2$	0
C	0	-1	0	$\pi_0(R_{d+5})$	0	0	0	$\mathbb{Z}$	$\mathbb{Z}_2$	$\mathbb{Z}_2$	0	$\mathbb{Z}$
CI	1	-1	1	$\pi_0(R_{d+6})$	0	0	$\mathbb{Z}$	$\mathbb{Z}_2$	$\mathbb{Z}_2$	0	$\mathbb{Z}$	0

absence of TP, CP, and chiral symmetry by taking into account additional chiral symmetry. The classification without additional chiral symmetry has been addressed in Ref. [57] where the symmetry classes are called AZ+$\mathcal{I}$ symmetry classes.

Here, we suppose d-dimensional systems to satisfy

$$
\{H(\boldsymbol{k}), \Sigma\} = 0, \tag{H1a}
$$

as well as constraints of each symmetry class. Here, the Hamiltonian preserving TP, CP, and chiral symmetry satisfies

$$
(TP)H(\boldsymbol{k})(TP)^{-1} = H(\boldsymbol{k}), \tag{H1b}
$$

$$
(CP)H(\boldsymbol{k})(CP)^{-1} = -H(\boldsymbol{k}), \tag{H1c}
$$

$$
\Gamma H(\boldsymbol{k})\Gamma^{-1} = -H(\boldsymbol{k}), \tag{H1d}
$$

where the operators of TP and CP transformations are antiunitary while the operator of the chiral transformation is unitary. We note that the operators TP, CP, and Γ defined above correspond to $\widetilde{TP}$, $\widetilde{CP}$, and $\widetilde{\Gamma}$ defined in Eq. (15). (In order to simplify the notation, we have omitted the tilde.)

In this section, we assume that the additional chiral symmetry satisfies the following relations:

$$
\{TP, \Sigma\} = 0, \tag{H2a}
$$

$$
[CP, \Sigma] = 0, \tag{H2b}
$$

$$
\{\Gamma, \Sigma\} = 0, \tag{H2c}
$$

which hold for the generic mechanical systems with friction (see Sec. IV B).

The classification results are summarized in Table III. In this table, we can see that the classification results for AZ+$\mathcal{I}$ symmetry classes with additional chiral symmetry are given by $\pi(C_{q+d})$ and $\pi(R_{q+d})$ while those for ordinary AZ symmetry classes are given by $\pi(C_{q-d})$ and $\pi(R_{q-d})$. This

TABLE IV. Classifying space and the corresponding homotopy $\pi_0(C_q)$ or $\pi_0(R_q)$.

Classifying space	$\pi_0(C_q)$ or $\pi_0(R_q)$
C_0	$\mathbb{Z}$
C_1	0
R_0	$\mathbb{Z}$
R_1	$\mathbb{Z}_2$
R_2	$\mathbb{Z}_2$
R_3	0
R_4	$\mathbb{Z}$
R_5	0
R_6	0
R_7	0

difference arises from the fact that the inversion flips the momentum $\boldsymbol{k} \to -\boldsymbol{k}$.

In the following, we see the details of the calculations.

1. Classification scheme

The topological classification of the Hermitian Hamiltonian is accomplished by the following steps [59].

(1) Deform the Hamiltonian into the gapped Dirac Hamiltonian

$$H = \sum_{j=1,\ldots,d} k_j \gamma_j + m\gamma_0. \qquad \text{(H3)}$$

Here, $\{\gamma_i, \gamma_j\} = 2\delta_{i,j}$ holds for $i, j = 0, \ldots, d$. When the Hamiltonian can be block diagonalized with an unitary operator, we consider the above Dirac Hamiltonian for each sector.

(2) Consider a Clifford algebra Cl_q or $Cl_{p,q}$ with symmetry operators and the matrices describing kinetic terms. Here, Cl_q denotes a complex Clifford algebra having q generators,

$$\{e_1, e_2, \ldots, e_q\}, \qquad \text{(H4)}$$

with $e_i^2 = 1$ for $i = 1, \ldots, q$. $Cl_{p,q}$ denotes a real Clifford algebra having $p + q$ generators,

$$\{e_1, \ldots, e_p; e_{p+1}, \ldots, e_{p+q}\}, \qquad \text{(H5)}$$

where p (q) generators square to -1 (1); $e_i^2 = 1$ (-1) for $i = 1, \ldots, p$ ($i = p + 1, \ldots, p + q$), respectively.
Because TP and CP transformations are described by antiunitary operators, we need to introduce an operator J to describe the complex structure in the presence of TP or CP symmetry (i.e., complex structure of real classes). Here, the operator J satisfies the relations $J^2 = -1$, $\{TP, J\} = \{CP, J\} = [H(\boldsymbol{k}), J] = 0$.

(3) Consider the extension problem by adding the mass term γ_0 in order to obtain the corresponding classifying space. When the extension problem is written as $Cl_q \to Cl_{q+1}$ ($Cl_{p,q} \to Cl_{p,q+1}$), the corresponding classifying space is C_q [R_{q-p}], respectively.
We note that when the extension problem is written as $Cl_{p,q} \to Cl_{p+1,q}$, the corresponding classifying space is R_{2+p-q}.

(4) Obtain the classification result $\pi_0(C_q)$ [$\pi_0(R_q)$]. Here, we use the fact listed in Table IV. We note that the Bott periodicity holds: $\pi_0(C_q) = \pi_0(C_{q+2})$ and $\pi_0(R_q) = \pi_0(R_{q+8})$.

In the following, we apply the above scheme to each case of AZ+$\mathcal{I}$ symmetry classes with additional chiral symmetry.

2. Application to systems of AZ+$\mathcal{I}$ classes with additional chiral symmetry

a. Class A

In this case, the Hamiltonian satisfies

$$\{H(\boldsymbol{k}), \Sigma\} = 0. \qquad \text{(H6)}$$

Thus, with the kinetic terms and the symmetry operator, we can consider a Clifford algebra with the following generators:

$$\{\gamma_1, \ldots, \gamma_d, \Sigma\}. \qquad \text{(H7)}$$

Introducing the mass term, the extension problem is written as $Cl_{1+d} \to Cl_{2+d}$ where Cl_{2+d} has generators

$$\{\gamma_0, \gamma_1, \ldots, \gamma_d, \Sigma\}. \qquad \text{(H8)}$$

Thus, the corresponding classifying space is C_{1+d}, which results in the classification result $\pi_0(C_{1+d})$.

b. Class AIII

In this case, the Hamiltonian satisfies

$$\{H(\boldsymbol{k}), \Sigma\} = 0, \qquad \text{(H9a)}$$

$$\{H(\boldsymbol{k}), \Gamma\} = 0. \qquad \text{(H9b)}$$

In addition, Σ and Γ anticommute with each other [see Eq. (H2c)].

Because the product $U = i\Gamma\Sigma$ ($U^2 = 1$) commutes with the Hamiltonian, one can block diagonalize the system into the ± 1 sector of U. The relations $\{U, \Sigma\} = \{U, \Gamma\} = 0$ indicate that applying Σ or Γ exchanges the plus and minus sectors. In other words, no symmetry is closed for each sector. Thus, we can classify the mass terms of the block-diagonalized Hamiltonian with the classifying space for the extension problem $Cl_d \to Cl_{1+d}$ where Cl_{1+d} has generators

$$\{\gamma_0, \gamma_1, \ldots, \gamma_d\}. \qquad \text{(H10)}$$

Therefore, the classification result is $\pi_0(C_d)$.

c. Classes AI and AII

In this case, the Hamiltonian satisfies

$$(TP)H(\boldsymbol{k})(TP)^{-1} = H(\boldsymbol{k}), \qquad \text{(H11a)}$$

$$\Sigma H(\boldsymbol{k})\Sigma^{-1} = -H(\boldsymbol{k}), \qquad \text{(H11b)}$$

with the anticommutation relation of TP and Σ [see Eq. (H2a)]. Noticing the relation $(TP)k_j\gamma_j(TP)^{-1} = k_j\gamma_j$ for $j = 1, \ldots, d$, we have $(TP)\gamma_j(TP)^{-1} = \gamma_j$.

Thus, for class AI [$(TP)^2 = 1$], the classifying space for the extension problem is written as $Cl_{d,3} \to Cl_{d+1,3}$ where $Cl_{d+1,3}$ is given by

$$\{J\gamma_0, J\gamma_1, \ldots, J\gamma_d; TP, JTP, \Sigma\}. \qquad \text{(H12)}$$

Thus, the corresponding classifying space is R_{d-1}.

In a similar way, we can obtain the classifying space for class AII [$(TP)^2 = -1$]. The extension problem is written as

$Cl_{d+2,1} \rightarrow Cl_{d+3,1}$ where $Cl_{d+3,1}$ has generators

$$\{J\gamma_0, TP, JTP, J\gamma_1, \ldots, J\gamma_d; \Sigma\}. \quad (H13)$$

Thus, the corresponding classifying space is R_{d+3}.

Therefore, we obtain the classification results $\pi_0(R_{d+7})$ and $\pi_0(R_{d+3})$ for classes AI and AII, respectively. Here, we have used the Bott periodicity $\pi_0(R_d) = \pi_0(R_{d+8})$.

d. Classes D and C

In this case, the Hamiltonian satisfies

$$(CP)H(\mathbf{k})(CP)^{-1} = -H(\mathbf{k}), \quad (H14a)$$

$$\Sigma H(\mathbf{k})\Sigma^{-1} = -H(\mathbf{k}), \quad (H14b)$$

with the commutation relation of CP and Σ [see Eq. (H2b)]. Noticing the relation $(CP)k_j\gamma_j(CP)^{-1} = -k_j\gamma_j$ for $j = 1, \ldots, d$, we have $(CP)\gamma_j(CP)^{-1} = -\gamma_j$.

Thus, for class D [$(CP)^2 = 1$], the extension problem is written as $Cl_{1,2+d} \rightarrow Cl_{1,3+d}$ where $Cl_{1,3+d}$ has generators

$$\{J\Sigma; \gamma_0, \gamma_1, \ldots, \gamma_d, CP, JCP\}. \quad (H15)$$

Thus, the corresponding classifying space is R_{d+1}.

In a similar way, we can obtain the classifying space for class C [$(CP)^2 = -1$]. The extension problem is written as $Cl_{3,d} \rightarrow Cl_{3,1+d}$ where $Cl_{3,1+d}$ has generators

$$\{CP, JCP, J\Sigma; \gamma_0, \gamma_1, \ldots, \gamma_d\}. \quad (H16)$$

Thus, the corresponding classifying space is R_{d-3}.

Therefore, we obtain the classification results $\pi_0(R_{d+1})$ [$\pi_0(R_{d+5})$] for class D (C), respectively. Here, we have used the Bott periodicity $\pi_0(R_d) = \pi_0(R_{d+8})$.

e. Classes BDI, DIII, CII, and CI

In this case, the Hamiltonian satisfies

$$(TP)H(\mathbf{k})(TP)^{-1} = H(\mathbf{k}), \quad (H17a)$$

$$(CP)H(\mathbf{k})(CP)^{-1} = -H(\mathbf{k}), \quad (H17b)$$

$$\Sigma H(\mathbf{k})\Sigma^{-1} = -H(\mathbf{k}) \quad (H17c)$$

with Σ anticommuting with TP and commuting with CP [see Eqs. (H2a) and (H2b)].

For class BDI [$(TP)^2 = (CP)^2 = 1$], the extension problem is written as $Cl_{1+d,3} \rightarrow Cl_{2+d,3}$ where $Cl_{2+d,3}$ has generators

$$\{JTC, J\gamma_0, J\gamma_1, \ldots, J\gamma_d; TP, JTP, \Sigma\}. \quad (H18)$$

Thus, the corresponding classifying space is R_d.

For class DIII [$(TP)^2 = -1$ and $(CP)^2 = 1$], the extension problem is written as $Cl_{2+d,2} \rightarrow Cl_{3+d,2}$ where $Cl_{3+d,2}$ has generators

$$\{TP, JTP, J\gamma_0, J\gamma_1, \ldots, J\gamma_d; JTC, \Sigma\}. \quad (H19)$$

Thus, the corresponding classifying space is R_{d+2}.

For class CII [$(TP)^2 = -1$ and $(CP)^2 = -1$], the extension problem is written as $Cl_{3+d,1} \rightarrow Cl_{4+d,1}$ where $Cl_{4+d,1}$ has generators

$$\{TP, JTP, JTC, J\gamma_0, J\gamma_1, \ldots, J\gamma_d; \Sigma\}. \quad (H20)$$

Thus, the corresponding classifying space is R_{d+4}.

TABLE V. Classification results for Hermitian systems of AZ+$\mathcal{I}$ symmetry classes with additional chiral symmetry and CP' symmetry. The "0" in the second, third, and fourth columns denotes that the corresponding symmetry is absent. The ± 1 in the second (the third) column represents the sign of $(TP)^2 = \pm 1$ [$(CP)^2 = \pm 1$], respectively. In the presence of TP symmetry, the symmetry class is CII$_+$ or CI$_+$ (CII$_-$ or CI$_-$) when the additional symmetry satisfies $[CP, CP'] = 0$ ($\{CP, CP'\} = 0$), respectively.

	TP	CP	Γ	Homotopy	$d=0$	1	2	3	4	5	6	7
C	0	-1	0	$\pi_0(C_{d+1})$	0	$\mathbb{Z}$	0	$\mathbb{Z}$	0	$\mathbb{Z}$	0	$\mathbb{Z}$
CII$_+$	-1	-1	1	$\pi_0(C_d)$	$\mathbb{Z}$	0	$\mathbb{Z}$	0	$\mathbb{Z}$	0	$\mathbb{Z}$	0
CI$_+$	1	-1	1	$\pi_0(C_d)$	$\mathbb{Z}$	0	$\mathbb{Z}$	0	$\mathbb{Z}$	0	$\mathbb{Z}$	0
CII$_-$	-1	-1	1	$\pi_0(R_{d+3})$	0	$\mathbb{Z}$	0	0	0	$\mathbb{Z}$	$\mathbb{Z}_2$	$\mathbb{Z}_2$
CI$_-$	1	-1	1	$\pi_0(R_{d+7})$	0	$\mathbb{Z}$	$\mathbb{Z}_2$	$\mathbb{Z}_2$	0	$\mathbb{Z}$	0	0

For class CI [$(TP)^2 = 1$ and $(CP)^2 = -1$], the extension problem is written as $Cl_{d,4} \rightarrow Cl_{1+d,4}$ where $Cl_{1+d,4}$ has generators

$$\{J\gamma_0, J\gamma_1, \ldots, J\gamma_d; TP, JTP, JTC, \Sigma\}. \quad (H21)$$

Thus, the corresponding classifying space is R_{d-2}.

From the above calculation, we obtain the classification results; for classes BDI, DIII, CII, and CI, we see $\pi_0(R_d)$, $\pi_0(R_{d+2})$, $\pi_0(R_{d+4})$, and $\pi_0(R_{d+6})$, respectively. Here, we have used the Bott periodicity $\pi_0(R_d) = \pi_0(R_{d+8})$.

3. Application to the symmetry classes CII, C, and CI with additional chiral symmetry and CP' symmetry

As discussed in Sec. IV B, mechanical systems, preserving particle-hole symmetry [$(CP)^2 = -1$], possess additional particle-hole symmetry CP' with $(CP')^2 = 1$ which commutes with Σ. Thus, we need to address the classification of the Hermitian Hamiltonian by taking into account these two types of particle-hole symmetry.

The classification results are summarized in Table V. By a proper choice of gauge, we can see that the operators CP and CP' satisfy the commutation or the anticommutation relation, and that both of CP and CP' commute with TP. The subscript of symmetry class indicates the commutation ($[CP, CP'] = 0$) or anticommutation ($\{CP, CP'\} = 0$) relation, e.g., for class CII$_+$, the commutation relation ($[CP, CP'] = 0$) holds. Here, the classification result for each case is obtained by assuming

$$[CP', \Sigma] = 0, \quad (H22)$$

as well as Eq. (H2). We note that generic mechanical systems satisfy these relations

In the following we discuss the details.

a. Class C

We note that a proper choice of gauge results in $[CP, CP'] = 0$ in the absence of the time-reversal symmetry. Thus, we address the classification for $[CP, CP'] = 0$.

In this case, the Hamiltonian satisfies the following relations:

$$(CP)H(\boldsymbol{k})(CP)^{-1} = -H(\boldsymbol{k}), \tag{H23a}$$

$$\Sigma H(\boldsymbol{k})\Sigma^{-1} = -H(\boldsymbol{k}), \tag{H23b}$$

$$UH(\boldsymbol{k})U^{-1} = H(\boldsymbol{k}), \tag{H23c}$$

with $U = CPCP'$. Here, we note that the following relations hold:

$$U^2 = -1, \tag{H24a}$$

$$[U, CP] = 0, \tag{H24b}$$

$$[U, \Sigma] = 0. \tag{H24c}$$

Because Eq. (H23c) holds, the Hamiltonian can be block diagonalized with the $\pm i$ sector of U. Applying the CP transformation exchanges the $\pm i$ sector while the chiral symmetry is closed for each sector.

Therefore, the mass terms of the block-diagonalized Hamiltonian are classified as follows. For each sector of U, the extension problem is written as $Cl_{1+d} \to Cl_{2+d}$ where Cl_{2+d} has generators

$$\{\Sigma, \gamma_0, \gamma_1, \dots, \gamma_d\}. \tag{H25}$$

Thus, the classifying space for the above extension problem is C_{1+d}. Noticing that CP transformation maps the Hamiltonian of $-i$ sector to that of $+i$ sector, we obtain the classification result $\pi_0(C_{1+d})$.

b. Class CII$_+$

For symmetry class CII$_+$ where $[CP, CP'] = 0$ holds, the following symmetry constraints are satisfied:

$$(TP)H(\boldsymbol{k})(TP)^{-1} = -H(\boldsymbol{k}), \tag{H26a}$$

$$\Gamma H(\boldsymbol{k})\Gamma^{-1} = -H(\boldsymbol{k}), \tag{H26b}$$

$$\Sigma H(\boldsymbol{k})\Sigma^{-1} = -H(\boldsymbol{k}), \tag{H26c}$$

$$UH(\boldsymbol{k})U^{-1} = H(\boldsymbol{k}), \tag{H26d}$$

with $U = CPCP'$ ($U^2 = -1$) and $\Gamma = TPCP$.

Defining $V = \Gamma\Sigma$ with $V^2 = -1$ [see Eq. (H2)], we have the following set of the operators:

$$[V, U] = 0, \tag{H27a}$$

$$\{V, TP\} = 0, \tag{H27b}$$

$$\{V, \Gamma\} = 0, \tag{H27c}$$

$$[U, TP] = 0, \tag{H27d}$$

$$[U, \Gamma] = 0, \tag{H27e}$$

$$[\Gamma, TP] = 0, \tag{H27f}$$

where unitary matrices U and V commute with the Hamiltonian.

Thus, the Hamiltonian can be block diagonalized with U and V. Each sector is labeled with the set of eigenvalues (u, v) where $u = \pm i$ ($v = \pm i$) denotes eigenvalue of U (V), respectively. Equations (H27b) and (H27d) indicate that applying the operator TP maps (u, v) sector to $(-u, v)$ sector. Equations (H27c) and (H27e) indicate that applying the operator Γ maps

(u, v) sector to $(u, -v)$ sector. These facts indicate that no symmetry is closed for each sector.

Therefore, the mass terms of the block-diagonalized Hamiltonian are classified as follows. For each sector, the extension problem is written as $Cl_d \to Cl_{1+d}$ where Cl_{1+d} has generators

$$\{\gamma_0, \gamma_1, \dots, \gamma_d\}. \tag{H28}$$

Thus, the classifying space for the above extension problem is C_d. Noticing that applying TP or Γ maps the Hamiltonian of (i, i) sector to that of the other sectors, we obtain the classification result $\pi_0(C_d)$.

c. Class CI$_+$

We consider the case where $(TP)^2 = 1$ and $\{CP, CP'\} = 0$ holds. Defining $\Gamma = iTPCP$ ($\Gamma^2 = 1$), we have Eq. (H26). We note that

$$[V, TP] = 0, \tag{H29a}$$

$$\{\Gamma, TP\} = 0 \tag{H29b}$$

hold instead of Eqs. (H27b) and (H27f). The other relations in Eq. (H27) hold.

In this case, the Hamiltonian can be block diagonalized for (u, v) sectors where $u = \pm i$ ($v = \pm i$) denotes eigenvalue of U (V), respectively. Equations (H27d) and (H29a) indicate that applying the operator TP flips sign both of u and v. Equations (H27c) and (H27e) indicate that applying the operator Γ flips sign of v.

Therefore, the mass terms of the block-diagonalized Hamiltonian are classified as follows. For each sector, the extension problem is written as $Cl_d \to Cl_{1+d}$ where Cl_{1+d} has generators

$$\{\gamma_0, \gamma_1, \dots, \gamma_d\}. \tag{H30}$$

Thus, the classifying space for the above extension problem is C_d. Noticing that applying TP or Γ maps the Hamiltonian of the (i, i) sector to that of the other sectors, we obtain the classification result $\pi_0(C_d)$.

d. Class CII$_-$

We consider the case where the Hamiltonian satisfies Eq. (H26) with $U = CPCP'$ ($U^2 = 1$) and $\{CP, CP'\} = 0$. In this case, the operators satisfy the following relations:

$$[U, TP] = 0, \tag{H31a}$$

$$\{U, \Gamma\} = 0, \tag{H31b}$$

$$\{U, V\} = 0, \tag{H31c}$$

$$\{V, TP\} = 0, \tag{H31d}$$

$$\{V, \Gamma\} = 0, \tag{H31e}$$

with $\Gamma = TPCP$ and $V = \Gamma\Sigma$ ($V^2 = -1$).

Thus, the Hamiltonian can be block diagonalized with U. We can see that applying Γ or V exchanges the plus and the minus sectors, while the TP symmetry is closed for each sector [see Eq. (H31)]. Namely, the block-diagonalized Hamiltonian preserves the symmetry of Σ and TP.

Therefore, the mass terms of the block-diagonalized Hamiltonian are classified as follows. For each sector, the

extension problem is written as $Cl_{2+d,1} \to Cl_{3+d,1}$, where $Cl_{3+d,1}$ has generators

$$\{TP, JTP, J\gamma_0, J\gamma_1, \ldots, J\gamma_d; \Sigma\}. \tag{H32}$$

Thus, the classifying space for the above extension problem is R_{d+3}. Noticing that applying Γ maps the Hamiltonian of the i sector to that of the other sector, we obtain the classification result $\pi_0(R_{d+3})$.

e. Class CI₋

We consider the case where $(TP)^2 = 1$ and $\{CP, CP'\} = 0$ hold. With $\Gamma = iTPTC$ and $U = CPCP'$ ($U^2 = 1$), we can see that the Hamiltonian satisfies Eq. (H26).

In this case, we obtain the classification results in a similar way to the previous case. First, we note that

$$[V, TP] = 0 \tag{H33}$$

holds instead of Eq. (H31d). The other relations of Eq. (H31) hold. Thus, block diagonalizing the Hamiltonian with U, we can see that applying Γ or V exchanges the plus and the minus sectors, while the TP symmetry is closed for each sector [see Eq. (H31)]. Namely, the block-diagonalized Hamiltonian preserves the symmetry of Σ and TP.

Therefore, the mass terms of the block-diagonalized Hamiltonian are classified as follows. For each sector, the extension problem is written as $Cl_{d,3} \to Cl_{1+d,3}$, where $Cl_{1+d,3}$ has generators

$$\{J\gamma_0, J\gamma_1, \ldots, J\gamma_d; TP, JTP, \Sigma\}. \tag{H34}$$

Thus, the classifying space for the above extension problem is R_{d+7}. Noticing that applying Γ maps the Hamiltonian of the plus sector to that of the other sector, we obtain the classification result $\pi_0(R_{d+7})$.

[1] C. L. Kane and E. J. Mele, Phys. Rev. Lett. **95**, 146802 (2005).
[2] B. A. Bernevig, T. L. Hughes, and S.-C. Zhang, Science **314**, 1757 (2006).
[3] M. König, S. Wiedmann, C. Brüne, A. Roth, H. Buhmann, L. W. Molenkamp, X.-L. Qi, and S.-C. Zhang, Science **318**, 766 (2007).
[4] M. Z. Hasan and C. L. Kane, Rev. Mod. Phys. **82**, 3045 (2010).
[5] X.-L. Qi and S.-C. Zhang, Rev. Mod. Phys. **83**, 1057 (2011).
[6] C. L. Kane and T. C. Lubensky, Nat. Phys. **10**, 39 (2013).
[7] T. Kariyado and Y. Hatsugai, Sci. Rep. **5**, 18107 (2015).
[8] R. Süsstrunk and S. D. Huber, Proc. Natl. Acad. Sci. USA **113**, E4767 (2016).
[9] F. D. M. Haldane and S. Raghu, Phys. Rev. Lett. **100**, 013904 (2008).
[10] S. Raghu and F. D. M. Haldane, Phys. Rev. A **78**, 033834 (2008).
[11] Z. Wang, Y. Chong, J. D. Joannopoulos, and M. Soljacic, Nature (London) **461**, 772 (2009).
[12] J. Ningyuan, C. Owens, A. Sommer, D. Schuster, and J. Simon, Phys. Rev. X **5**, 021031 (2015).
[13] V. V. Albert, L. I. Glazman, and L. Jiang, Phys. Rev. Lett. **114**, 173902 (2015).
[14] C. H. Lee, S. Imhof, C. Berger, F. Bayer, J. Brehm, L. W. Molenkamp, T. Kiessling, and R. Thomale, Commun. Phys. **1**, 39 (2018).
[15] D. J. Thouless, M. Kohmoto, M. P. Nightingale, and M. den Nijs, Phys. Rev. Lett. **49**, 405 (1982).
[16] B. I. Halperin, Phys. Rev. B **25**, 2185 (1982).
[17] Y. Hatsugai, Phys. Rev. Lett. **71**, 3697 (1993).
[18] J.-X. Fu, R.-J. Liu, and Z.-Y. Li, Appl. Phys. Lett. **97**, 041112 (2010).
[19] N. Hatano and D. R. Nelson, Phys. Rev. Lett. **77**, 570 (1996).
[20] C. M. Bender and S. Boettcher, Phys. Rev. Lett. **80**, 5243 (1998).
[21] T. Fukui and N. Kawakami, Phys. Rev. B **58**, 16051 (1998).
[22] T. E. Lee, Phys. Rev. Lett. **116**, 133903 (2016).
[23] Y. Xu, S.-T. Wang, and L.-M. Duan, Phys. Rev. Lett. **118**, 045701 (2017).

[24] Z. Gong, S. Higashikawa, and M. Ueda, Phys. Rev. Lett. **118**, 200401 (2017).
[25] H. Shen, B. Zhen, and L. Fu, Phys. Rev. Lett. **120**, 146402 (2018).
[26] J. Carlström and E. J. Bergholtz, Phys. Rev. A **98**, 042114 (2018).
[27] A. Guo, G. J. Salamo, D. Duchesne, R. Morandotti, M. Volatier-Ravat, V. Aimez, G. A. Siviloglou, and D. N. Christodoulides, Phys. Rev. Lett. **103**, 093902 (2009).
[28] C. E. Rüter, K. G. Makris, R. El-Ganainy, D. N. Christodoulides, M. Segev, and D. Kip, Nat. Phys. **6**, 192 (2010).
[29] A. Regensburger, C. Bersch, M.-A. Miri, G. Onishchukov, D. N. Christodoulides, and U. Peschel, Nature (London) **488**, 167 (2012).
[30] B. Zhen, C. W. Hsu, Y. Igarashi, L. Lu, I. Kaminer, A. Pick, S.-L. Chua, J. D. Joannopoulos, and M. Soljacic, Nature (London) **525**, 354 (2015).
[31] A. U. Hassan, B. Zhen, M. Soljačić, M. Khajavikhan, and D. N. Christodoulides, Phys. Rev. Lett. **118**, 093002 (2017).
[32] H. Zhou, C. Peng, Y. Yoon, C. W. Hsu, K. A. Nelson, L. Fu, J. D. Joannopoulos, M. Soljačić, and B. Zhen, Science **359**, 1009 (2018).
[33] A. Ghatak and T. Das, J. Phys.: Condens. Matter **31**, 263001 (2019).
[34] V. Kozii and L. Fu, arXiv:1708.05841.
[35] T. Yoshida, R. Peters, and N. Kawakami, Phys. Rev. B **98**, 035141 (2018).
[36] H. Shen and L. Fu, Phys. Rev. Lett. **121**, 026403 (2018).
[37] V. M. Martinez Alvarez, J. E. Barrios Vargas, and L. E. F. Foa Torres, Phys. Rev. B **97**, 121401(R) (2018).
[38] S. Yao and Z. Wang, Phys. Rev. Lett. **121**, 086803 (2018).
[39] S. Yao, F. Song, and Z. Wang, Phys. Rev. Lett. **121**, 136802 (2018).
[40] F. K. Kunst, E. Edvardsson, J. C. Budich, and E. J. Bergholtz, Phys. Rev. Lett. **121**, 026808 (2018).
[41] E. Edvardsson, F. K. Kunst, and E. J. Bergholtz, Phys. Rev. B **99**, 081302(R) (2019).

[42] D. S. Borgnia, A. J. Kruchkov, and R.-J. Slager, arXiv:1902.07217.

[43] Z. Gong, Y. Ashida, K. Kawabata, K. Takasan, S. Higashikawa, and M. Ueda, Phys. Rev. X **8**, 031079 (2018).

[44] K. Kawabata, S. Higashikawa, Z. Gong, Y. Ashida, and M. Ueda, Nat. Commun. **10**, 297 (2019).

[45] K. Kawabata, K. Shiozaki, M. Ueda, and M. Sato, arXiv:1812.09133.

[46] J. C. Budich, J. Carlström, F. K. Kunst, and E. J. Bergholtz, Phys. Rev. B **99**, 041406(R) (2019).

[47] R. Okugawa and T. Yokoyama, Phys. Rev. B **99**, 041202(R) (2019).

[48] T. Yoshida, R. Peters, N. Kawakami, and Y. Hatsugai, Phys. Rev. B **99**, 121101(R) (2019).

[49] T. Katō, *Perturbation Theory for Linear Operators*, Vol. 132 (Springer, Berlin, 1966).

[50] K. Takata and M. Notomi, Phys. Rev. Lett. **121**, 213902 (2018).

[51] T. Takata and M. Notomi (private communication).

[52] In order to satisfy $U_\Gamma^2 = \sigma_0$, the projected operator U_Γ takes $U_\Gamma = \boldsymbol{n} \cdot \boldsymbol{\sigma}$ or σ_0. However, when $U_\Gamma = \sigma_0$, the projected Hamiltonian becomes anti-Hermitian whose eigenvalues are always pure imaginary.

[53] We note that when $b = d = 0$ holds, the Hamiltonian is not defective. However, this condition is not satisfied without fine tuning.

[54] This is because the eigenvalues are written as $-ib/2 \pm \sqrt{\omega_{0n}^2 - (b/2)^2}$, which can be seen in a similar way as Eq. (E4). Here, ω_{0n} denotes the eigenvalue of the Hamiltonian for $b = 0$.

[55] The band touching occurs when the two bands touch in the complex plane because the Hamiltonian is non-Hermitian.

[56] K. Kawabata, T. Bessho, and M. Sato, Phys. Rev. Lett. **123**, 066405 (2019).

[57] T. Bzdušek and M. Sigrist, Phys. Rev. B **96**, 155105 (2017).

[58] The block-diagonalized Hamiltonian for the $\pm$ sector is written as $H_\pm = b_{00}\tau_0 + b_{01}\tau_1 \pm b_{22}\tau_2 + id_{03}\tau_3$.

[59] T. Morimoto and A. Furusaki, Phys. Rev. B **88**, 125129 (2013).